**TECHNISCHE
UNIVERSITÄT
WIEN**
Vienna University of Technology

DIPLOMARBEIT

The Electronic Structure of Transition Metal Oxides - A Comparison between Hybrid and On-Site Corrected Density Functional Calculations for Bulk and Monolayer Systems

**Ausgeführt am Institut für Angewandte Physik
der Technische Universität Wien**

**unter der Anleitung von
Ao.Univ.Prof. Dipl.-Ing. Dr.techn. Josef Redinger**

durch

Michael Wolloch

Juchgasse 34/11, 1030 Wien

Wien, am 7.1.2011   _____

Abstract

In the present diploma thesis, the eight $3d$ transition metal monoxides ScO, TiO, VO, CrO, MnO, FeO, CoO and NiO were studied in the ideal rocksalt structure. The Vienna Ab-initio Simulation Package (VASP) was used to solve the Kohn–Sham equations of Density Functional Theory (DFT) selfconsistently within the framework of the Projector-Augmented Wave method (PAW). The compounds presented above are considered to be prototypes of systems containing localized electrons, for which exchange and correlation effects are not sufficiently described by the Local Density Approximation (LDA), or the semilocal Generalized Gradient Approximation (GGA). All eight monoxides were studied in an antiferromagnetic configuration, in bulk as well as in a (100) monolayer, which, to our best knowledge, was not done before.

The Hartree–Fock hybrid functional HSE06 was used to create a benchmark lattice constant and density of states (DOS) graph for each system. In the following attempts were made to reproduce the HSE06 lattice constants and DOS peaks with a computationally much cheaper method by adding an on-site repulsion term for the $3d$ electrons to the LDA. This approach is known as the LDA+U method. To find the right value for the parameter U, the DOS was dissected into Oxygen p, and transition metal d_{eg} and d_{t2g} states. The peak positions and bandwidths were used as characteristic fitting values, as well as the lattice constant. The parameter U was optimized for different sets of conditions by minimizing the mean quadratic deviation with respect to the HSE06 calculation. In order to create a bandgap, or enlarge the already existing gap to its hybrid functional counterpart, another parameter, the scissor shift Δ, was calculated. While being in the same order of magnitude, values for the on-site interaction parameter U are often quite different, depending on the chosen set of fitting attributes. For bulk CrO, the ideal values of U are for example found to be: 0.0 eV for the valence bandwidth, 1.2 eV for the lattice constant, 2.9 eV for all parameters and 4.6 eV for the peak positions. The spread is usually smaller in the case of the (100) monolayer, with an overall increased U. This was to be expected, as the restrictive geometry forces the electrons even closer together.

This work provides a large dataset of U and Δ values for the gradually filling $3d$ shell. It also indicates in which cases the approximation of the HSE06 calculation with the LDA+U+Δ works well and in which it does not. The monolayer calculations allow to extrapolate the change of these parameters for real surface layers in a slab.

Kurzfassung

In der vorliegenden Diplomarbeit wurden die acht $3d$ Übergangsmetalloxide ScO, TiO, VO, CrO, MnO, FeO, CoO und NiO, in der idealen Kochsalzstruktur analysiert. Um die auf der Dichtefunktionaltheorie (DFT) aufbauenden Kohn–Sham Gleichungen zu lösen, kam das Vienna Ab-initio Simulation Package (VASP) genannte Programmpaket zum Einsatz, wobei das Verhalten der Elektronen im Potential der Atomrümpfe mit der Projector Augmented Wave Methode (PAW) beschrieben wurde. Die oben genannten Verbindungen gelten als Prototypen für Systeme mit stark lokalisierten Elektronen, für die die gängigen Näherungen für die Austausch- und Korrelationswechselwirkung nur bedingt sinnvoll anwendbar sind. Diese üblichen Funktionale sind die Lokale Dichtenäherung (LDA) und die um den Gradienten der örtlichen Dichte erweiterte, semilokale "Generalized Gradient Approximation" (GGA). Alle acht Verbindungen wurden in antiferromagnetischer Konfiguration sowohl im unendlich ausgedehnten Kristall, als auch in einer (100) Monolage untersucht, was zu unserem besten Wissen bisher noch nicht versucht wurde.

Das Hartree–Fock Hybridfunktional HSE06 wurde verwendet um für jede Verbindung eine Referenzgitterkonstante und einen Referenzgraphen der Denity of States (DOS) zu bestimmen. Es wurde versucht diese Attribute mit einer, die Rechenzeit betreffend, viel günstigeren Methode zu imitieren, bei der zur LDA ein weiterer Term hinzugefügt wird (LDA+U), der eine lokale, abstoßende Wirkung auf die $3d$ Elektronen beschreibt. Um den Parameter U zu bestimmen wurden die DOS Graphen in einen Sauerstoff p, sowie in Übergangsmetall d_{eg} und d_{t2g} Teile aufgespalten. Die Positionen der einzelnen Peaks dieser Teile, die Bandbreiten und die Gitterkonstante wurden als Parameter herangezogen. Der Wert von U wurde nun dahingehend optimiert, dass der mittlere quadratische Fehler, in Bezug zu den HSE06 Referenzen, für verschiedene Gruppen von Attributen minimalisiert wurde. Um die Bandstruktur besser anzupassen wurde zusätzlich eine Parameter Δ berechnet, der den Abstand von Valenz- zu Leitungsband, also die Bandlücke, korrigieren kann.

Obwohl grundsätzlich von gleicher Größenordnung können die genauen Werte von U für eine Verbindung beträchtlich variieren, je nachdem für welchen Parameter optimiert wurde. So sind die idealen Werte für CrO zum Beispiel 0.0 eV für die Valenzbandbreite, 1.2 eV für die Gitterkonstante, 2.9 eV wenn alle Parameter berücksichtigt werden und 4.6 eV für die Peak Positionen. Diese Abweichungen sind für die Monolagen nach unseren Berechnungen meist geringer, wobei aber ein insgesamt höheres U zur Anpassung

benötigt wird. Dies ist nicht verwunderlich, da die Elektronen durch die einschränkende Geometrie noch näher zusammengedrückt werden.

Diese Arbeit bietet einen guten Überblick über die verschiedenen Werte von U und Δ für die sich stetig auffüllende $3d$ Schale. Außerdem wird gezeigt in welchen Fällen die Annäherung an die HSE06 Methode mit dem LDA+U+Δ Konzept gut gelingt, und in welchen Fällen gröbere Abweichungen in Kauf genommen werden müssen. Durch die Kenntnis der Werte für den unendlich ausgedehnten Kristall und die Monolage können Rückschlüsse auf die Parameter in verschiedenen Schichten einer realen Oberfläche gezogen werden.

Contents

1 Introduction

While Computational Material Science (CMS) is still a young field in condensed matter physics, ever increasing computer power and continuous advances in programming have made the "computer experiment" a popular choice for predicting results of experiments and testing theories. Ab initio calculations (in theory) do not require any other input, but the type of lattice and the atomic species used, as well as some fundamental constants.

Rather than solving immensely complicated many-body Schrödinger-equations, one may utilize the Density Functional Theory (DFT) to solve the electronic problem. This method, which will be described in more detail in section 2.1, deals with the electronic charge density and can, in theory, describe the exact groundstate of the examined system. However, the exact exchange and correlation terms are presently unknown, and several approximations have to be used. While the standard Local Density Approximation (LDA), or its successor, the Generalized Gradient Approximation (GGA) give usually good results, this is not the case for systems containing localized electrons, e.g. transition metals and their oxides. In the present work two DFT-based methods, a Hartree-Fock Hybrid Functional (HSE06) and the LDA+U approach, that uses an additional parameter U as a penalty function to the energy for localized electrons, are discussed (see sections 2.3 and 2.4) and compared (section 4). The aim of this effort is to model the computationally very expensive HSE method with the about a hundred times cheaper LDA+U approach.

Eight $3d$ transition metal monoxides (TMOs), ScO, TiO, VO, CrO, MgO, FeO, CoO and NiO, were studied in bulk as well as in a monolayer. All systems were set up in the ideal rocksalt structure, although in reality the structure of VO is distorted, TiO shows about 15% vacancies and Sc and Cr do not even exist as monoxides. This should not be considered to be a big problem, as the discussed compounds only serve as models for much larger systems, containing similar bonds between transition metals and oxygen. It is a reasonable guess, that the values of U found in this thesis should at least be good starting points for the electron exchange and correlation in other systems, which are too large to be treated with the HSE functional.

The structure of this work is ordered as follows. DFT, LDA, GGA, LDA+U and HSE, as well as the used program package VASP, are discussed briefly in section 2. A short

account of ferro- and antiferromagnetism, as well as a quick survey of the exchange and superexchange interaction, will be given in the third section. The main results of this work are presented in section 4, followed by a summary and conclusion in section 5.

2 Computational Methods

2.1 Density Functional Theory

As mentioned in section 1, Density Functional Theory, or DFT, is widely used in ab-initio calculations. The overview that is given here, is following [1]. The idea is based on the observation of Hohenberg and Kohn, that the information contained in a many-electron wave function of a given problem is in principle completely represented by the electron density ρ. The Hohenberg-Kohn theorem [2] states now, that the ground state energy is a functional of the electronic density $E[\rho]$, which is minimized at the density $\rho(\vec{r}) = \rho_0(\vec{r})$. This theorem can be proven in an elegant way (see [3]).

To obtain the functional, which is equal to the expectation value $\langle \Phi | H | \Phi \rangle$, were Φ denotes the many-body wave function, one usually splits it into four parts, expressing the kinetic energy, the ionic potential, the Hartree term and the exchange and correlation term.

$$E[\rho] = E_{kin}[\rho] + E_{ion}[\rho] + E_{Hartree}[\rho] + E_{xc}[\rho] \qquad (2.1)$$

Now one strives to express these terms through the electron density, which is easily done for the ionic potential and the Hartree term:

$$E_{ion}[\rho] = \int d^3r \, V_{ion}(\vec{r})\rho(\vec{r}) \qquad (2.2)$$

$$E_{Hartree}[\rho] = \frac{1}{2} \int d^3r' \int d^3r \, \frac{\rho(\vec{r'})\rho(\vec{r})}{|\vec{r} - \vec{r'}|} \qquad (2.3)$$

At this point it is interesting to observe that $E[\rho] - E_{ion}[\rho]$ is a universal functional, which does only depend on the number of electrons in the system, but not on the ionic potential. This means, that, if the exact expression for E_{xc} could be found (it will be shown that the E_{kin} term does not make any trouble) all materials could be solved by simply adding the adequate potential. Unfortunately, no exact representations for the exchange-correlation term is known so one is forced to use one of several approximations.

To circumvent the difficulties in expressing the kinetic energy through ρ, Kohn and Sham [4] introduced auxiliary single-electron orbitals $\varphi_i(\vec{r})$, which form exactly the same charge density.

$$\rho(\vec{r}) = \sum_{i=1}^{N} |\varphi_i(\vec{r})|^2 \qquad (2.4)$$

With the new functions $\varphi_i(\vec{r})$, the kinetic energy now yields

$$E_{kin} = \sum_i \int d^3r \, \frac{\hbar^2}{2m} (\nabla \varphi_i(\vec{r}))^2 \quad . \qquad (2.5)$$

For calculating the energy and density of the ground state, one has to minimize the energy functional $E[\rho]$ with respect to ρ

$$\frac{\delta\{E[\rho] - \mu(\int d^3r \, \rho(\vec{r}) - N)\}}{\delta\rho(\vec{r})} = 0 \qquad (2.6)$$

where the Lagrange parameter μ fixes the number of electrons to N. This equation can now be transformed to minimize with respect to the φ_i instead of ρ, whereupon ε_i ensures the normalization of the functions φ_i.

$$\frac{\delta\{E[\rho] - \varepsilon_i(\int d^3r \, |\varphi_i(\vec{r})|^2 - 1)\}}{\delta\varphi_i(\vec{r})} = 0 \qquad (2.7)$$

The result leads to the Kohn-Sham equations [4],

$$\left[-\frac{\hbar^2}{2m_e}\Delta + V_{ion}(\vec{r}) + \int d^3r' \frac{\rho(\vec{r'})}{|\vec{r} - \vec{r'}|} + \frac{\delta E_{xc}[\rho]}{\delta\rho(\vec{r})} \right] \varphi_i(\vec{r}) = \varepsilon_i\varphi_i(\vec{r}) \qquad (2.8)$$

which are Schrödinger equations of single electrons moving in an effective (single-body) potential $V_{eff} = V_{ion} + V_H[\rho] + V_{xc}[\rho]$.

$$V_{eff}(\vec{r}) = V_{ion}(\vec{r}) + \int d^3r' \frac{\rho(\vec{r'})}{|\vec{r} - \vec{r'}|} + \frac{\delta E_{xc}[\rho]}{\rho(\vec{r})} \qquad (2.9)$$

The Kohn-Sham potential and the charge density could now be calculated selfconsistently, were it not for the unknown term E_{xc}. How approximations are found for the exchange and correlations will be shown in the next section.

2.2 LDA and GGA

The various Local Density Approximation (LDA) models are obtained by evaluating the correlation and exchange energy of the homogeneous electron gas at the density of the local non-homogeneous system. This is a good approximation for systems with a slowly varying charge density, which is true for s- and p-states, but should not work well for d- and f-electrons.

$$\epsilon_{xc}^{LDA}[\rho(\vec{r})] := \epsilon_{xc}^{hom}(\rho_0)|_{\rho_0 \to \rho(\vec{r})} \tag{2.10}$$

For spin-polarized calculations, one usually speaks of LSDA (Local Spin Density Approximation) and the prescription is carried out for $\rho_+(\vec{r})$ and $\rho_-(\vec{r})$. (Also frequently the parameterization $\rho(\vec{r}) = \rho_+(\vec{r}) + \rho_-(\vec{r})$ and $\zeta(\vec{r}) = \frac{1}{\rho(\vec{r})}(\rho_+(\vec{r}) - \rho_-(\vec{r}))$ is used.) For reasons of simplicity, these distinction shall not be made in this section, although nearly all calculations in the present work were spin-polarized.

The groundstate of a homogeneous electron gas against a uniform background of positive charge (the jellium model) can be solved with the Hartree–Fock approximation using plane waves. This yields an exchange term of fundamental constants, where V denotes the Volume, N the number of electrons and k_F the Fermi wavelength. (The solution for jellium can, for instance, be found in [5])

$$\epsilon_x^{LDA}(\rho_0) = -\frac{N}{V}\frac{3}{4}\frac{e^2 k_F}{\pi} = -\frac{3}{4}\left(\frac{3}{\pi}\right)^{\frac{1}{3}}e^2\rho_0^{\frac{4}{3}} = -C_x\,\rho_0^{\frac{4}{3}} \tag{2.11}$$

This result is the exchange energy per unit volume. The correlation contribution ϵ_c^{LDA} of the jellium density ρ_0 can be obtained e.g. from advanced many-body techniques like Quantum Monte Carlo. The approximated functional is now obtained by integrating $\epsilon_{xc}^{LDA} = \epsilon_x^{LDA} + \epsilon_c^{LDA}$.

$$E_{xc}[\rho] \overset{LDA}{\approx} \int d^3r \, \epsilon_{xc}^{LDA}(\rho_0 = \rho(\vec{r})) \qquad (2.12)$$

This can now be inserted into equation (2.8), which then can be solved selfconsistently.

Surprisingly, the LDA does not only work well in the slowly varying limit of the charge density, but also gives quite acceptable results for many other systems. Gunnarsson et al. showed [6], that the exchange-correlation hole modeled by the LDA does not have to be an exact facsimile of the true hole, but that it is sufficient that it provides a reasonable approximation of the spherical average of the real exchange correlation hole. Other reasons for the suprising success of the LDA as well as a detailed account of parameterizations can be found in [7].

The freedom to modify the exchange-correlation term however, has provoked a large amount of effort, culminating in the Generalized Gradient Approximations (GGA). The concept states that it should be possible to better the functional by adding derivative terms. The resulting functional still does not take non-local contributions into account, but by adding the gradients of the density one obtains a semilocal exchange-correlation term.

$$E_{xc}^{GGA}[\rho, \nabla\rho] = \int d^3r \, \epsilon_{xc}^{GGA}\left(\rho(\vec{r}), |\nabla\rho(\vec{r})|\right) \qquad (2.13)$$

In general, GGA, in comparison to LDA, tend to improve total energies and atomization energies [8]. It also softens bonds to correct [9] or overcorrect [10] the LDA and generally favors density inhomogeneity more than LDA does. There is no standard functional, but PW91 [11] by Perdew et al. and PBE [12] by Perdew, Burke and Ernzerhof, which was also utilized for the present work, are very commonly used. (There is also no standard functional for the LDA, but in that case variations in the parameterization are much smaller.)

2.3 Hartree–Fock Hybrid Functionals

Another way of treating electron-electron interactions in the context of DFT is to utilize the Hartree–Fock equation. One obtains the equation by means of the variational

principle that states, that wave functions which solve Schrödinger's equation are extrema of the functional $F_H[\psi] = \langle\psi|\hat{H}|\psi\rangle$, under the constraint that $\langle\psi|\psi\rangle = 1$. For the wave function $|\psi\rangle$ one now uses Slater determinants. The derivation of the actual equation can be found in many textbooks (e.g. [5]) and will not be given here. For our purpose it is sufficient to give the result of the coulomb interaction part of the expectation value of the Hamiltonian. (As the Hamiltonian is not spin-dependent, it is possible to give ψ the form $\psi_j(\vec{r_i}\sigma_i) = \varphi_j(\vec{r_i})\chi_j(\sigma_i)$, were χ_j is either "spin up" or "spin down".)

$$E_{xc} = \iint \frac{e^2\, d^3r_1\, d^3r_2}{|\vec{r_1} - \vec{r_2}|} \sum_{i<j} \left[|\varphi_i(\vec{r_1})|^2\, |\varphi_j(\vec{r_2})|^2\; -\; \varphi_i^*(\vec{r_1})\, \varphi_j^*(\vec{r_2})\, \varphi_i(\vec{r_2})\, \varphi_j(\vec{r_1})\, \delta_{\chi_i\chi_j} \right]$$

$$(2.14)$$

The first term is the coulomb integral, which also appears in the Hartree equation which does not use antisymmetrical wave functions. The second term is called the exchange integral. It is non-local and can be interpreted as two electrons switching places while interacting. The minus sign is a consequence of antisymmetry, while $\delta_{\chi_i\chi_j}$ is shorthand for $\sum_\sigma \chi_i(\sigma)\, \chi_j(\sigma)$.

In actual use not the whole exchange is taken from Hartree–Fock but a so called hybrid functional is constructed, mixing some Fock–exchange to the usual GGA term while correlation is treated exclusively by GGA.

$$E_{xc}^{hybr} \;=\; a\, E_x^{HF}\; +\; (1-a)\, E_x^{GGA}\; +\; E_c^{GGA} \tag{2.15}$$

The mixing coefficient a is determined from comparison with advanced many-body approaches. The hybrid method successfully delocalizes the exchange hole and presents a significant improvement over the GGA descriptions of molecular properties. However, until recently, calculation of the spatially decaying $\left(\frac{1}{r}\right)$ Fock-exchange in solids with periodic boundary conditions was nearly impossible, due to the vast amount of computing power needed. In 2003, Heyd, Scuseria and Ernzerhof proposed a new hybrid functional based on a screened Coulomb potential for the exchange [13], which distinguishes between short- and long-ranged parts of the interaction and circumvents this bottleneck. The GGA method used is PBE, and all other Coulomb interactions of the Hamiltonian, e.g. the repulsion of the electrons, are still treated with the full range

potential. The Coulomb operator $\frac{1}{r}$ for the exchange however, is split into a short- (SR) and a long-range (LR) part,

$$\frac{1}{r} = \underbrace{\frac{\text{erfc}(\omega r)}{r}}_{\text{SR}} + \underbrace{\frac{\text{erf}(\omega r)}{r}}_{\text{LR}} \tag{2.16}$$

where $\text{erfc}(\omega r) = 1 - \text{erf}(\omega r)$. The parameter ω is used to define the borderline between the short- and longe-range parts, where for $\omega = 0$ the SR part is equivalent to the full Coulomb operator and the LR part vanishes, while the opposite is true for $\omega \to \infty$. After splitting every term of equation 2.15 into a SR and a LR part, Heyd at al. found, that, for reasonable values of ω, the HF long-range exchange terms contribute quite little to this functional and may therefore be replaced by its PBE counterpart. Today, the originally functional by Heyd, Scuseria and Ernzerhof (HSE03) proposed in [13] is not commonly used, because a mistake in the code led to two different values for ω, for each HF and PBE respectively (see [14]). The tests and refinements carried out in 2006 in [15] fix ω to 0.2Å^{-1} and a to $\frac{1}{4}$ to form the HSE06 functional which is frequently used and was also applied in the present work.

$$E_{xc}^{HSE06} = \frac{1}{4} E_x^{HF,SR} + \frac{3}{4} E_x^{PBE,SR} + E_x^{PBE,LR} + E_c^{PBE} \tag{2.17}$$

2.4 LDA+U

A different approach to rid the LDA from its faults in strongly correlated systems is the usage of quasi atomic interactions for the localized d- or f-electrons. In 1991 Anisimov, Zaanen and Andersen proposed to incorporate an additional parameter U, as used in the Hubbard Hamiltonian, into the LDA [16]. The Hubbard model, devised in 1936, was originally developed to explain magnetic ordering and is an addition to the tight binding approximation, in which an energy penalty U is added for any atomic site occupied by more than one electron. In second quantization the Hubbard Hamiltonian reads

$$\hat{H} = \sum_{\langle ij \rangle \sigma} -\mathfrak{t} \left[\hat{c}_{i\sigma}^{\dagger} \hat{c}_{j\sigma} + \hat{c}_{j\sigma}^{\dagger} \hat{c}_{i\sigma} \right] + U \sum_{i} \hat{n}_{i\uparrow} \hat{n}_{i\downarrow} \tag{2.18}$$

where the sum $\langle ij \rangle$ is taken over distinct nearest neighbor pairs and $\mathbf{t}$ denotes the hopping integral.

Anisimov et al. argued that localization in the LDA is not controlled by a Hubbard U, but by the Stoner Parameter I, which represents the Hund's rule exchange and is typically one order of magnitude smaller than U. While in a homogenous electron gas spin dependence has its physical origin indeed in the Hund's rule exchange, this does not hold for strongly localized electrons. The functional provided by Anisimov and coworkers fixed this problem, but had the serious disadvantage of depending on the chosen orbital basis. This flaw was corrected by Liechtenstein, Anisimov and Zaanen in 1995 [17]. Their rotationally invariant LDA+U functional reads

$$E^{LDA+U}[\,\rho^\sigma, n^\sigma\,] \;=\; E^{LDA}[\,\rho^\sigma\,] \;+\; E^{U}[\,n^\sigma\,] \;-\; E_{dc}[\,n^\sigma\,] \quad , \qquad (2.19)$$

where $E^{LDA}[\rho^\sigma]$ is the standard functional dependent of the charge density of spin-σ electrons. $E^{U}[n^\sigma]$ denotes the orbital polarizations in a screened mean field (Hartree–Fock) way and n^σ is the density matrix for correlated electrons. The last term corrects for double counting, so that in the limit of vanishing orbital polarization, the functional is reduced to normal LDA. It is worth noting, that E^{U}, as well as E_{dc}, depend on the screened Coulomb parameter U and the screened exchange parameter J and that for a diagonal density matrix n^σ this approach is equivalent to the original LDA+U.

All this still leaves the question how to obtain the parameters U and J, that are necessary for practical calculations. In [16] a method is described to calculate U and J by applying a variety of constraints. To acquire for example the appropriate U for a d-electron, one has to remove the transfer integrals between the selected orbitals and the rest of the system. The d-occupancy is now varied (δn_d), while the other electrons are allowed to relax. It follows that

$$U \;=\; \frac{\delta^2 E_{tot}}{\delta n_d^2} \qquad\qquad (2.20)$$

with E_{tot} being the total LDA energy. More about this constrained LDA (CLDA) method and also about the GW approach [18] (G stands for Green's function and W for a dynamically screened Coulomb interaction) can be found in [19]. Several other

methods and variants for calculating the parameters U and J were developed recently (see e.g. [20, 21, 22]), but no "golden standard" has emerged yet, and results can be quite different. It is therefore often more practicable to leave the confines of the ab-initio approach and fit parameters consistently with experiments or different calculation methods such as HF hybrid functionals (see 2.3). Exactly this was done in the present thesis, using the LDA+U flavor of Dudarev et al. [23]. In this simplified approach, only the difference between U and J is relevant, and so only one parameter has to be varied to find optimal results.

$$E^{LDA+U} = E^{LDA} + \frac{(U-J)}{2} \sum_{\sigma} \left[\left(\sum_{m_1} n^{\sigma}_{m_1,m_1} \right) - \left(\sum_{m_1,m_2} \hat{n}^{\sigma}_{m_1,m_2} \hat{n}^{\sigma}_{m_2,m_1} \right) \right] \quad (2.21)$$

Again, n^{σ} denotes the on-site occupation matrix. The ansatz can be understood as adding a penalty functional to the LDA total energy, that leads the on site occupancy matrix in the direction of idempotency, i.e. $n^{\sigma} = n^{\sigma} n^{\sigma}$. Real matrices are only idempotent if their eigenvalues are either 0 or 1, corresponding to fully occupied or unoccupied states.

2.5 VASP

2.5.1 General Information

VASP is the abbreviation for Vienna Ab-initio Simulation Package [24, 25, 26, 27], which was used for all computions in this work. It is a complex program to perform ab-initio quantum-mechanical molecular dynamics simulations. The term ab-initio indicates that the calculation is from the ground up, using as only input the type of lattice and the atomic species, but no empirical data. VASP uses a plane wave basis set, periodic boundary conditions and can be operated with either ultrasoft pseudopotentials (US-PP [28, 29]) or the projector-augmented wave method (PAW [30, 31]) . It is based on DFT (see section 2.1) and it is possible to select a vast amount of different calculation schemes and options. Forces and the full stress tensor can be calculated with VASP and used to relax atoms into their instantaneous ground-state.

2.5.2 Input- and Output–Files

When working with VASP, one encounters numerous files which can be divided roughly in input- and output-files, even though several output files can be used as input for another calculation. None but the most essential files for this work shall be discussed here. These are: INCAR, POSCAR, POTCAR, KPOINTS, OUTCAR and DOSCAR.

- INCAR

  The INCAR file tells the program what to do and how to do it. Conveniently, most of the many selectable options have reasonable default values, that will work for many calculations, so one can often get by with defining just a few. In the given example, the tag ISPIN sets a spin polarized calculation and LHFCALC determines the use of Hartree-Fock like calculations while the screening tag HF-SCREEN, set to 0.2, selects the HSE06 functional. Lines that beginn with an exclamation mark are not read, so the ISIF tag, which would be set to 3, thus allowing the cell and the ions to relax in any way, is ignored and put to the default value 0, which allows the ions to relax, but keeps the cell as it is. But, as the ionic steps are set to 1 in the NSW tag, no relaxation can be performed anyway.

```
 SYSTEM = FeO bulk
 ISPIN = 2
 MAGMOM = 2.6 -2.6 2*0.0
 LORBIT = 11
!ISTART = 1
 ICHARG = 1
 LHFCALC = .TRUE. ; HFSCREEN = 0.2
 ALGO = DAMPED  ; TIME = 0.5
 ENCUTFOCK = 0
 NKRED = 2
!LREAL = A
 ISMEAR = 0
 NSW = 1
 IBRION = 1
!ISIF = 3
```

File 1: INCAR

- POSCAR

  In the POSCAR file, the VASP-user specifies the lattice vectors of the systems (lines 3 to 5), the lattice constant (line 2), the type and number of the ions (line 6 to 7) and finally, the initial positions of these ions, given either in cartesian or direct mode. (In cartesian mode, each position is scaled by the lattice constant

only, whereas in direct mode it is multiplied by the lattice vectors.) The first line in the file is a comment line and usually displays the systems name.

```
 FeO bulk AF rocksalt
   4.33000000000000
     1.0000000000000000     0.5000000000000000     0.5000000000000000
     0.5000000000000000     1.0000000000000000     0.5000000000000000
     0.5000000000000000     0.5000000000000000     1.0000000000000000
   Fe   O
   2   2
Cartesian
  0.0000000000000000  0.0000000000000000  0.0000000000000000
  1.0000000000000000  1.0000000000000000  1.0000000000000000
  0.5000000000000000  0.5000000000000000  0.5000000000000000
  1.5000000000000000  1.5000000000000000  1.5000000000000000
```

File 2: POSCAR

- POTCAR

  POTCAR files are provided for each atomic species with the VASP-package. They contain the pseudopotential as well as fundamental constants like mass, valance and energy in the reference configuration. There are several files (US-PP or PAW, LDA or PBE or PW91) for each element, which can be selected. If several atomic species are used in a calculation, the POTCAR files need to be joined together with the same ordering as the POSCAR file.

- KPOINTS

  As one might expect from the name the KPOINTS file deals with the coordinates, weights and mesh size of the k-point grid. The first line is treated as a comment, and one lets the mesh usually be generated automatically by VASP, by typing 0 in the second line. (Alternatively all k-points can be entered manually, or one generates 'strings' of k-points along high symmetry lines, which is usefull for band-structure calculations.) The third line specifies if the grid should be centered on the Γ point, or if a original Monkhorst-Pack scheme should be used. The fourth line set the number of subdivisions along the reciprocal latticevector, defining the refinement of the mesh. The fifth line corresponds to an optional shift in the grid.

```
 Automatic
 0   ! automatic generation
Gamma
 10 10 10
  0  0  0
```

File 3: KPOINTS

- OUTCAR

  This file is composed of (nearly) all relevant output of a VASP run. The resulting energy, magnetic moments, charge distribution, bandstructure, stress tensor and much more can be found here. The file is usually a couple of thousend lines long, so only a short section near the end is printed here. If one is only interested in the resulting energy and how quick the results converge, one can also use the more accessible OSZICAR file.

```
 magnetization (x)

# of ion    s       p       d      tot
------------------------------------------
   1      0.006   0.005   3.620   3.630
   2     -0.006  -0.005  -3.620  -3.630
   3      0.000   0.000   0.000   0.000
   4      0.000   0.000   0.000   0.000
------------------------------------------
tot       0.000   0.000   0.000   0.000




--------------------------------------------------------------------------------------------------



  FREE ENERGIE OF THE ION-ELECTRON SYSTEM (eV)
  -------------------------------------------------
  free   energy   TOTEN  =       -46.965139 eV

  energy  without entropy=       -46.965139  energy(sigma->0) =      -46.965139

    FORLOC: cpu time    0.00: real time    0.00
    FORHF : cpu time 1641.67: real time 1641.82
    FORNL : cpu time    0.47: real time    0.47
    FORCOR: cpu time    2.33: real time    2.33

 VOLUME and BASIS-vectors are now :
 --------------------------------------------------------------------------------
 energy-cutoff  :      400.00
 volume of cell :       40.59
     direct lattice vectors                 reciprocal lattice vectors
    4.330000000  2.165000000  2.165000000    0.346420323 -0.115473441 -0.115473441
    2.165000000  4.330000000  2.165000000   -0.115473441  0.346420323 -0.115473441
    2.165000000  2.165000000  4.330000000   -0.115473441 -0.115473441  0.346420323

 length of vectors
    5.303145293  5.303145293  5.303145293    0.382982077  0.382982077  0.382982077
```

File 4: OUTCAR

- DOSCAR

  The DOSCAR file contains the density of states (DOS) as well as the integrated DOS. A header (containing the energy range and the Fermi energy) is followed by five columns showing: Energy, DOS(up), DOS(down), integrated DOS(up),

integrated DOS(down). If a PAW potential is used and the LORBIT tag in the INCAR file is greater than 10, there are additional 19 columns for each ion. In these, the partial DOS for each orbital (s, py, pz, px, dxy, dyz, dz^2, dxz and dx^2) for each spin are mapped against the energy.

For more information about VASP in general and the different VASP files, listed or not listed in this section, please consult [32]

2.5.3 Setup for Calculations

The calculations in the present thesis are performed with the VASP package using the PAW potentials with the PBE functional [12]. For all transition metals, all but the $3d$ and $4s$ states are frozen in the core potential, but for Chromium, Vanadium and Titanium the $3p$ states and for Scandium, both $3p$ and $3s$ orbitals were considered as valence states. For the Oxygen ions, $2s$ and $2p$ electrons were used. The Hartree-Fock hybrid calculations were performed with settings equivalent to the HSE06 [15] functional and for the LDA+U runs, the approach by Dudarev [23] was used. The plain wave energy cutoff was usually 400 eV, but was increased to 600 eV if relaxations were performed.

3 Ferro- and Antiferromagnetism

Although magnetism is known since ancient times (Thales of Milet, about 625-564 b.c., wrote about a stone that could attract iron), microscopic theories on magnetism were not presented before the late 19th century. Ferromognetism was first explained in 1907 by Weiss in his molecular field model, but the physical origin of this molecular field, was not known at that time. The reason for the slow development in magnetism physics lies in the solely quantum mechanical origin of magnetic effects in solids. In the following subsections, the molecular field model of Weiss will be discussed. After that, a brief description of the quantum mechanical reason for the molecular field, the exchange interaction, is given. The more complicated situation in transition metal oxides is governed by the superexchange process, which will be discussed afterwards. The whole section closely follows the book [33] by Peter Mohn.

3.1 Weiss Molecular Field Model

In his 1907 work [34], Weiss proposed the existence of an internal magnetic field, H_M, responsible for spontaneous magnetic order. It consists of a proportionality factor N and the magnetization M.

$$H_M = NM \qquad (3.1)$$

It is therefore assumed, that the interaction between the spins, leading to magnetic order, has the form of a uniform field. While the temperature dependence of the magnetization is calculated by classical mechanics, quantum theoretical principles enter by the assumption of discrete energies, associated with the quantum number m_J. For a particle with quantum numbers J and m_J, the magnetic moment is

$$\mu = m_J g_j \mu_B \,, \qquad \text{for} \quad -J \leq m \leq +J \qquad (3.2)$$

where g_j is the Landé factor and μ_B is the Bohr magneton. It arises, because the magnetic moment is not simply the sum of angular and spin component, but one has to take the different gyromagnetic factors ($g_l = -1$ and $g_s = -2.0023$, here approximated

to $g_s = -2$) into account.

$$g_j = -\frac{3J(J+1) - L(L+1) + S(S+1)}{2J(J+1)} \tag{3.3}$$

Following classical mechanics, the magnetization M at given temperature T is given by the statistical average over all possible states of m_J.

$$\frac{M}{M_0} = \frac{1}{Jg_j\mu_B} \frac{\sum_{m_J=-J}^{+J} m_J g_j \mu_B \, e^{-\frac{W}{k_B T}}}{\sum_{m_J=-J}^{+J} e^{-\frac{W}{k_B T}}} \tag{3.4}$$

In equation (3.4), $W = -m_J g_j \mu_B H$ and H consists of the molecular field plus an external field H_{ext}, while M_0 is the magnetic moment at $T = 0$. To calculate this expression, one introduces abbreviations

$$a = \frac{Jg_j\mu_B H}{k_B T} \quad , \qquad x = e^{\frac{a}{J}} = e^{\frac{g_j \mu_B H}{k_B T}} \tag{3.5}$$

thus producing

$$\frac{M}{M_0} = J^{-1} \frac{\sum_{-J}^{+J} m_J x^{m_J}}{\sum_{-J}^{+J} x^{m_J}} \quad . \tag{3.6}$$

Now, one can rewrite the fraction of the sums given above using the derivative.

$$\frac{\sum m_J x^{m_J}}{\sum x^{m_J}} = x \frac{\frac{\mathrm{d}}{\mathrm{d}x} \sum x^{m_J}}{\sum x^{m_J}} = x \frac{\mathrm{d}}{\mathrm{d}x} \ln \sum x^{m_J} \tag{3.7}$$

The result of the sum of x_J^m from $-J$ to J is known and one can take the logarithm and then carry out the calculation

$$\sum_{-J}^{+J} x^{m_J} = \frac{x^{-J}\left(1 - x^{2J+1}\right)}{1-x} = \frac{x^{-J} - x^{J+1}}{1-x} \quad ,$$

$$\ln \sum x^{m_J} = \ln\left(x^{-J} - x^{J+1}\right) - \ln\left(1 - x\right) \quad ,$$

$$
\begin{aligned}
x\frac{\mathrm{d}}{\mathrm{d}x}\ln\sum x^{m_J} \;=\;& \frac{-Jx^{-J}-(J+1)\,x^{J+1}}{x^{-J}-x^{J+1}}+\frac{x}{1-x}\\[2mm]
=\;& \frac{-J\left(x^{-J}+x^{J+1}\right)}{x^{-J}-x^{J+1}}-\frac{x^{J+1}}{x^{-J}-x^{J+1}}+\frac{x}{1-x}\\[2mm]
=\;& \frac{J\left(x^{2J+1}+1\right)}{\left(x^{2J+1}-1\right)}-\frac{x^{J+1}}{x^{-J}-x^{J+1}}-\frac{x}{x-1}\\[2mm]
=\;& \frac{J\left(x^{2J+1}+1\right)}{\left(x^{2J+1}-1\right)}\\[2mm]
&+\frac{1}{2}\left(\frac{x^{J+1}+x^{-J}+x^{J+1}-x^{J}}{x^{J+1}-x^{-J}}-\frac{x+1+x-1}{x-1}\right)\\[2mm]
=\;& \left(J+\frac{1}{2}\right)\frac{x^{2J+1}+1}{x^{2J+1}-1}-\frac{1}{2}\left(\frac{x+1}{x-1}\right)\quad.
\end{aligned}
$$

Now the final result is obtained by resubstituting the abbreviations and using the identity $\coth x = \frac{e^{2x}-1}{e^{2x}+1}$.

$$
\frac{M}{M_0}=B\left(a,J\right)=\frac{2J+1}{2J}\coth\left(a\frac{2J+1}{2J}\right)-\frac{1}{2J}\coth\left(\frac{a}{2J}\right)\quad,\tag{3.8}
$$

where $B(a,J)$ denotes the Brillouin function.

To calculate an expression for the Curie temperature T_{c}, one can approximate the coth in the limit of high temperatures ($a<<1$).

$$
\coth x = \frac{1}{x}+\frac{x}{3}-\ldots\tag{3.9}
$$

This yields a much easier form of the Brillouin function

$$
B(a,J)\cong\frac{1}{3}\,a\left(\frac{J+1}{J}\right)\quad.\tag{3.10}
$$

Now, one simply inserts a, sets $H_{ext}=0$, uses $H_M=NM$ and solves for $k_{\mathrm{B}}T_{\mathrm{c}}$.

$$
\begin{aligned}
\frac{M}{M_0}\;=\;& \frac{1}{3}\frac{J+1}{J}\frac{Jg_J\mu_{\mathrm{B}}}{k_{\mathrm{B}}T}NM\quad,\\[2mm]
\Rightarrow\quad k_{\mathrm{B}}T_{\mathrm{c}}\;=\;& \frac{1}{3}\left(J+1\right)g_J\mu_{\mathrm{B}}NM_0\tag{3.11}
\end{aligned}
$$

This result can be further simplified for electrons, where $J = S = \frac{1}{2}$ and $|g_j| = 2$.

$$k_{\mathrm{B}}T_{\mathrm{c}} = \mu_{\mathrm{B}} N M_0 \tag{3.12}$$

Now the molecular field constant can be calculated if experimental results for μ_{B} and T_{c} are inserted into (3.12).

	$N\ (\mathrm{T}/\mu_{\mathrm{B}})$	$H_{\mathrm{M}}\ (\mathrm{T})$
Fe	700	1500
Co	1300	2100
Ni	1600	940

Table 1: Molecular field constant N and respective molecular field H_M for Fe, Co and Ni. After P. Mohn [33]

The calculated fields (see table 1), are much larger than one would expect of a magnetic interaction. The magnitude of this fields lies in the nature of the exchange interaction, that is responsible for it. It will be discussed in section 3.2.

For paramagnetic systems, the molecular field constant N is zero and the susceptibility can be calculated by differentiating M with respect to H_{ext}.

$$\chi = \frac{1}{3}J(J+1)\frac{g_j^2\mu_{\mathrm{B}}^2}{k_{\mathrm{B}}T} = \frac{\mu_J^2}{3k_{\mathrm{B}}T} \tag{3.13}$$

The quantum mechanical value of the magnetic moment due to the angular momentum J is

$$\mu_J^2 = J(J+1)g_j^2\mu_{\mathrm{B}}^2 = \mu_{\mathrm{eff}}^2 \quad . \tag{3.14}$$

Here, an effective moment μ_{eff} is defined, that can be calculated by measuring the Curie constant (3.16). It gives the size of local magnetic moments above the Curie temperature. For itinerant magnetic moments, it is not well defined.

For the calculation of the susceptibility in ferromagnetic systems above the Curie temperature T_{c} one uses equation (3.11).

$$
\begin{aligned}
\frac{M}{M_0} &= \frac{1}{3}\frac{J+1}{J}\frac{Jg_j\mu_\text{B}}{k_\text{B}T}\left(H_\text{ext}+NM\right) \\
&= \frac{1}{3}\frac{J+1}{J}\frac{Jg_j\mu_\text{B}}{k_\text{B}T}\left(H_\text{ext}+\frac{3k_\text{B}T_\text{c}M}{(J+1)\,g_j\mu_\text{B}M_0}\right) \quad, \\
\Rightarrow \quad \frac{M}{M_0}\left(1-\frac{T_\text{c}}{T}\right) &= \frac{1}{3}\frac{(J+1)\,g_j\mu_\text{B}}{k_\text{B}T}H_\text{ext} \quad, \\
\Rightarrow \quad \chi = \frac{M}{H_\text{ext}} &= \frac{C}{T-T_\text{c}} \quad,\quad \text{with}\quad C = \frac{1}{3}\left(J+1\right)\frac{g_j\mu_\text{B}}{k_\text{B}}M_0 \quad. \quad (3.15)
\end{aligned}
$$

This relation is the Curie-Weiss law. The general expression for the Curie Constant

$$
C = \frac{\mu_\text{eff}^2}{3k_\text{B}} \quad. \tag{3.16}
$$

is found by using the definitions for μ_eff (3.14) and M_0 (3.4). For $J = S = \frac{1}{2}$ and $|g_j| = 2$, C is reduced to $\frac{\mu_\text{B}M_0}{k_\text{B}}$. All systems follow the linear temperature dependence of the inverse susceptibility χ^{-1} for high enough temperatures, as it is the classical limit.

The spontaneous magnetization as a function of temperature is also given by the Brillouin function. Using equation (3.1) and (3.11) to transform a in equation (3.8), one gets

$$
\frac{M}{M_0} = B\left(\frac{3J}{J+1}\frac{M}{M_0}\frac{T_\text{c}}{T},J\right) \quad, \tag{3.17}
$$

which again for $J = S = \frac{1}{2}$ and $|g_j| = 2$ gives

$$
\frac{M}{M_0} = \tanh\left(\frac{M}{M_0}\frac{T_\text{c}}{T}\right) \quad. \tag{3.18}
$$

Using the classical limit $J = \infty$, one finally gets an expression known as the Langevin function.

$$
\frac{M}{M_0} = \coth\left(a\right) - \frac{1}{a} \quad. \tag{3.19}
$$

Equation (3.19) is a transcendental equation which is usually solved graphically or numerically. However, approximate solutions can be found around $T = 0$ and $T = T_\text{c}$. Expanding (3.19) around T_c one immediately obtains the mean field exponent $\beta = \frac{1}{2}$

$$
\frac{M}{M_0} = \left(3\left(\frac{T_\text{c}}{T}-1\right)\right)^{\frac{1}{2}} \simeq \left(\frac{T_\text{c}}{T}-1\right)^{\beta} \quad. \tag{3.20}
$$

This is a universal relation between the magnetization M and the temperature T, but unfortunately it does not work satisfactorily for metals and alloys. The critical exponent $\beta = \frac{1}{2}$ differs from experiment, were it is found to be approximately 0.33. In systems with weak interaction between individual spins however, the Weiss model works well. Expanding (3.19) around $T = 0$ gives

$$\frac{M}{M_0} = 1 - 2e^{\left(-\frac{2T_c}{T}\right)} \quad . \tag{3.21}$$

Finally it should be said, that this mean field model is only valid in the case of localized magnetic moments and fails for itinerant electrons, except in the high temperature regime, were the classical limit is reached. Also, the temperature dependence is more often given by a power law, than the complex relation in (3.18).

3.2 The Exchange Interaction

The molecular field, that Weiss used to describe ferromagnetism in 1907, was at that time a somewhat arbitrary construct and it was not clear what kind of interaction should produce such strong fields. In 1919, Miss van Leeuwen proved in her Ph.D. thesis, that for any dynamical system rigorous application of statistical mechanics must lead to zero susceptibility [35]. Therefore it was clear, that magnetic order had to stem from quantum mechanical origins.

The term exchange interaction comes from the original formulation of the Hartree–Fock theory, where it is one of two integrals, that describe electron–electron interaction (see also 2.3). In a general form the exchange integral can be written as

$$J = \int \varphi_1^*(\vec{r}_2)\,\varphi_2^*(\vec{r}_1)\,W(\vec{r}_1, \vec{r}_2)\,\varphi_1(\vec{r}_1)\,\varphi_2(\vec{r}_2)\,\mathrm{d}^3 r_1\,\mathrm{d}^3 r_2 \quad , \tag{3.22}$$

with W being an exchange operator (e.g. the Coulomb operator $\frac{1}{|r_1 - r_2|}$). It is called the exchange integral, because two electrons switch places during the interaction. An easy way to understand the exchange interaction and its connection to magnetism is the Heitler–London theory of the H_2 molecule. It shall be reviewed in the next section.

3.2.1 Heitler–London Theory of the Exchange Field

In 1927, Walter Heitler and Fritz London presented their solution of the H_2 molecule [36]. There they considered the electron spin and the Pauli principle, resulting in anti-symmetric wavefunctions. Their approach was a linear combination of atomic orbitals (LCAO) and so results are only valid for localized electrons.

One starts with Schrödinger's equation of the system containing two protons (at the sites a and b) and two electrons (at sites 1 and 2). The distance between the protons shall be r_{ab}, the distance between the electrons r_{12} and the distances between the electrons and the protons r_{a1}, r_{b1}, r_{a2} and r_{b2}, respectively.

$$\left(-\frac{\hbar^2}{2m_e} \left(\nabla_1^2 + \nabla_2^2 \right) + \left[\frac{e^2}{r_{ab}} - \frac{e^2}{r_{a1}} - \frac{e^2}{r_{a2}} - \frac{e^2}{r_{b1}} - \frac{e^2}{r_{b2}} + \frac{e^2}{r_{12}} \right] \right) \Psi_m = U_m \Psi \quad (3.23)$$

U_m is the exact eigenvalue for the molecular wavefunction Ψ_m. For two separated H atoms, the groundstates ($1s$), wavefunctions (ψ_{a1} and ψ_{b2}) and the eigenvalues (both times E_0) are known. In the molecule, the groundstate would be four times degenerate, if the electron-electron interaction would not be considered, because each electron can have either spin up ($\alpha = \frac{1}{2}$) or spin down ($\beta = -\frac{1}{2}$). U_m would be $2E_0$.

If the electron-electron interaction is taken into account the molecular wavefunction Ψ_m can no longer be calculated analytically. The usual way to solve this problem is to set up a sum of known wavefunctions, furnish these with coefficients and then use these coefficients as variational parameters to minimize the total energy. In the case of the H_2 molecule, one constructs out of the four wavefunctions, $\psi_{a\alpha}$, $\psi_{a\beta}$, $\psi_{b\alpha}$ and $\psi_{b\beta}$, four slater determinants to satisfy the antisymmetry condition.

$$\Psi_1 = \begin{vmatrix} \psi_a \alpha \, (1) & \psi_b \alpha \, (1) \\ \psi_a \alpha \, (2) & \psi_b \alpha \, (2) \end{vmatrix} \quad \Rightarrow M_\mathrm{S} = 1 \quad , \quad (3.24)$$

$$\Psi_2 = \begin{vmatrix} \psi_a \beta \, (1) & \psi_b \alpha \, (1) \\ \psi_a \beta \, (2) & \psi_b \alpha \, (2) \end{vmatrix} \quad \Rightarrow M_\mathrm{S} = 0 \quad , \quad (3.25)$$

$$\Psi_3 = \begin{vmatrix} \psi_a \alpha \, (1) & \psi_b \beta \, (1) \\ \psi_a \alpha \, (2) & \psi_b \beta \, (2) \end{vmatrix} \quad \Rightarrow M_\mathrm{S} = 0 \quad , \quad (3.26)$$

$$\Psi_4 = \begin{vmatrix} \psi_a \beta \, (1) & \psi_b \beta \, (1) \\ \psi_a \beta \, (2) & \psi_b \beta \, (2) \end{vmatrix} \quad \Rightarrow M_\mathrm{S} = -1 \quad . \quad (3.27)$$

As shown in the following, the degenerate groundstate is now split into a spin singlet
($S = 0$, $M_S = 0$) and a triplet ($S = 1$, $M_S = -1, 0, +1$). The triplet is "ferromagnetic",
with two parallel spins, while the singlet is "antiferromagnetic", with antiparallel spins.
At the moment it is not clear which one is going to be the groundstate, and how large
the energy splitting is going to be.

Since one started from isolated atoms, an orthogonality relation between the electronic
wavefunction is easily written down,

$$S_{\alpha\beta} = \int \psi_a \alpha \psi_b \beta d\tau = 0 \quad , \tag{3.28}$$

$$S_{\alpha\alpha} = \int \psi_a \alpha \psi_b \alpha d\tau = S_{\beta\beta} = \int \psi_a \beta \psi_b \beta d\tau = S \quad , \tag{3.29}$$

and the overlap integral S is directly related to it. Two cases are possible

$$r_{ab} = 0 \Rightarrow S = 1 \quad \text{the wavefunctions are identical,}$$

$$r_{ab} \rightarrow \infty \Rightarrow S = 0 \quad \text{no overlap.}$$

A linear combination of the slater determinants Ψ_i is used to construct an approximation wave function for the molecule. The coefficients c_i are later used as variational parameters.

$$\Psi = \sum_{i=1}^{4} c_i \Psi_i \tag{3.30}$$

To calculate the Hamiltonian for this wavefunction, a number of abbreviations are introduced.

$$\mathcal{H}\Psi = U\Psi \quad ,$$

$$\text{with} \quad \mathcal{H} = 2E_0 + V_0 \quad ,$$

$$\text{and} \quad V_0 = e^2 \left[\frac{1}{r_{ab}} - \frac{1}{r_{a2}} - \frac{1}{r_{b1}} + \frac{1}{r_{12}} \right] \quad .$$

Note, that the eigenvalue U of the approximate wavefunction is not the exact solution

U_m. It is also convenient to introduce the following spin functions

$$
\begin{aligned}
\sigma_1 &= \alpha\,(1)\,\alpha\,(2) & \mathcal{M}_S = +1 & \quad , \\
\sigma_2 &= \beta\,(1)\,\alpha\,(2) & \mathcal{M}_S = 0 & \quad , \\
\sigma_3 &= \alpha\,(1)\,\beta\,(2) & \mathcal{M}_S = 0 & \quad , \\
\sigma_4 &= \beta\,(1)\,\beta\,(2) & \mathcal{M}_S = -1 & \quad .
\end{aligned}
$$

Now the Schrödinger equation (3.23) can be rewritten in a more compact form.

$$
(U - 2E_0)\,\Psi - V_0\Psi = 0 \tag{3.31}
$$

Multiplying (3.31) with the product $\psi_a\alpha\,(1)\,\psi_b\beta\,(2)$ form the right yields

$$
(U - 2E_0) \int_\sigma \alpha\,(1)\,\beta\,(2)\,\mathrm{d}\sigma \int_\tau \Psi\,\psi_a\,(1)\,\psi_b\,(2)\,\mathrm{d}\tau
$$
$$
= \int_\sigma \alpha\,(1)\,\beta\,(2)\,\mathrm{d}\sigma \int_\tau \Psi\,V_0\,\psi_a\,(1)\,\psi_b\,(2)\,\mathrm{d}\tau \quad ,
$$

or in general

$$
(U - 2E_0) \int_\sigma \sigma_k\mathrm{d}\sigma \int_\tau \Psi\,\psi_a\,(1)\,\psi_b\,(2)\,\mathrm{d}\tau = \int_\sigma \sigma_k\mathrm{d}\sigma \int_\tau \Psi\,V_0\,\psi_a\,(1)\,\psi_b\,(2)\,\mathrm{d}\tau . \tag{3.32}
$$

One can now replace Ψ with the sum in (3.30) and obtain

$$
\sum_{i=1}^4 c_i\,[H_{ik} + (2E_0 - U)\,S_{ik}] = 0 \quad , \tag{3.33}
$$

where
$$
S_{ik} = \int_\sigma \sigma_k\mathrm{d}\sigma \int_\tau \Psi_i\,\psi_a\,(1)\,\psi_b\,(2)\,\mathrm{d}\tau \quad , \tag{3.34}
$$

and
$$
H_{ik} = \int_\sigma \sigma_k\mathrm{d}\sigma \int_\tau \Psi_i\,V_0\,\psi_a\,(1)\,\psi_b\,(2)\,\mathrm{d}\tau \quad . \tag{3.35}
$$

Both indices, i and k, run from one to four. Now one can vary the total energy with

respect to the coefficient c_i, which leads to a block diagonal matrix determinant.

$$\begin{vmatrix} H_{11} + ES_{11} & 0 & 0 & 0 \\ 0 & H_{22} + ES_{22} & H_{23} + ES_{23} & 0 \\ 0 & H_{32} + ES_{32} & H_{33} + ES_{33} & 0 \\ 0 & 0 & 0 & H_{44} + ES_{44} \end{vmatrix} = 0 \quad , \qquad (3.36)$$

with $E = 2E_0 - U$. While the block in the center has to be diagonalized first, the first and the last element have the same form, and can be calculated immediately. They both have S $= 1$ and give "ferromagnetic" solutions with parallel spins. For the first element ($S_{11} \to \mathcal{M}_S = +1$, $i = 1$, $k = 1$), both electrons have spin "up", and for the last, ($S_{11} \to \mathcal{M}_S = -1$, $i = 4$, $k = 4$), they have both spin "down". The calculation of the first element is now shown explicitly:

$$\Psi_1 = \sigma_1 \left[\psi_a (1) \psi_b (2) - \psi_a (2) \psi_b (1) \right] \quad ,$$

$$S_{11} = \underbrace{\underbrace{\int_\sigma \sigma_1^2 d\sigma}_{=1} \int_\tau \psi_a (1) \psi_b (2) \psi_a (1) \psi_b (2) \, d\tau}_{=1}$$

$$- \underbrace{\underbrace{\int_\sigma \sigma_1^2 d\sigma}_{=1} \int_\tau \psi_a (2) \psi_b (1) \psi_a (1) \psi_b (2) \, d\tau}_{=S^2} \quad ,$$

$$S_{11} = 1 - S^2 \quad , \tag{3.37}$$

$$H_{11} = \underbrace{\underbrace{\int_\sigma \sigma_1^2 d\sigma}_{=1} \int_\tau |\psi_a (1)|^2 |\psi_b (2)|^2 V_0 d\tau}_{=C}$$

$$- \underbrace{\underbrace{\int_\sigma \sigma_1^2 d\sigma}_{=1} \int_\tau \psi_a (2) \psi_b (1) \psi_a (1) \psi_b (2) V_0 d\tau}_{=J} \quad ,$$

$$H_{11} = C - J \quad . \tag{3.38}$$

Here S is the overlap, C the coulomb, and J the exchange integral. The first matrix

element is now given by

$$H_{11} + (2E_0 - U) S_{11} = 0 \quad ,$$
$$\Rightarrow \quad U = U_1 = 2E_0 + \frac{C - J}{1 - S^2} \quad , \quad \mathcal{M}_S = +1 \quad . \quad (3.39)$$

U_4 is calculated analogously and yields the same value as U_1. For the diagonalization of the center block of (3.36), one can use the following relations, which stem from the fact, that the matrix is hermitian.

$$S_{22} = S_{33} = \int_\sigma \sigma_2^2 \mathrm{d}\sigma \int_\tau |\psi_a(1)|^2 |\psi_b(2)|^2 \mathrm{d}\tau = 1 \quad , \qquad (3.40)$$

$$H_{22} = H_{33} = \int_\sigma \sigma_2^2 \mathrm{d}\sigma \int_\tau |\psi_a(1)|^2 |\psi_b(2)|^2 V_0 \mathrm{d}\tau = C \quad , \qquad (3.41)$$

$$S_{23} = S_{32} = \int_\sigma \sigma_3^2 \mathrm{d}\sigma \int_\tau \psi_a(2) \psi_b(1) \psi_a(1) \psi_b(2) \mathrm{d}\tau = S^2 \quad , \qquad (3.42)$$

$$H_{23} = H_{32} = \int_\sigma \sigma_3^2 \mathrm{d}\sigma \int_\tau \psi_a(2) \psi_b(1) \psi_a(1) \psi_b(2) V_0 \mathrm{d}\tau = J \quad , \qquad (3.43)$$

With this, the block can be rewritten to

$$\begin{vmatrix} C + (2E_0 - U) & J + (2E_0 - U) S^2 \\ J + (2E_0 - U) S^2 & C + (2E_0 - U) \end{vmatrix} = 0 \quad ,$$

which leads to the eigenvalues

$$U_2 = 2E_0 + \frac{C + J}{1 + S^2} \quad , \quad \mathcal{M}_S = 0 \quad , \quad \mathcal{S} = 0 \quad , \qquad (3.44)$$

and

$$U_3 = 2E_0 + \frac{C - J}{1 - S^2} \quad , \quad \mathcal{M}_S = 0 \quad , \quad \mathcal{S} = 1 \quad . \qquad (3.45)$$

The solution for U_3 is equal to the solutions for U_1 and U_4, therefore, the Heitler–London model for the H_2 molecule produces two energy states. One triplet state with $\mathcal{S} = 1$ and $\mathcal{M}_S = -1, 0, +1$ for U_4, U_3 and U_1, respectively, and one singlet with $\mathcal{S} = 0$ and $\mathcal{M}_S = 0$ for U_2. The singlet has antiparallel spins and represents the "antiferromagnetic" solution. If the wavefunction overlap S is small, the relations for

the triplet and the singlet are simplified to

$$U_{\text{triplet}} = 2E_0 + C - J \tag{3.46}$$

$$U_{\text{singlet}} = 2E_0 + C + J \tag{3.47}$$

From this it is clear, that the sign of the exchange integral J is responsible for ferro-or antiferromagnetic order. If $J > 0$, the ferromagnetic state is the groundstate, for $J < 0$ the antiferromagnetic is. In the case of the H_2 molecule, the singlet state is the groundstate, as it is indeed for all systems containing two fermions with non–pathological potential. The theorem which proofs this fact is usually attributed to Wigner and can be reviewed, as well as an extension for n-electron systems, in [37]. Also, the unphysical large molecular fields in the theory of Weiss is explainable now. The magnitude of the exchange interaction is, in the approximation of vanishing overlap, $2J$ and J is an interaction of Coulomb type. The origin of the molecular field is therefore of electrostatic, rather than of magnetic nature.

3.2.2 Exchange in Larger Systems – The Heisenberg Model

This section contains a short glance on the Heisenberg model [38, 39], and shall serve as an additional viewpoint on the connection of the exchange interaction and magnetism for more than two electrons. A complete overview of the model is not even attempted, but can be found in many textbooks (e.g. [33, 40]).

The famous quantum mechanical Heisenberg Hamiltonian in its simplest form

$$\mathcal{H} = J \sum_{\langle i,j \rangle} \mathbf{S}_i \, \mathbf{S}_j \quad , \tag{3.48}$$

can be viewed as the operater for the exactly half filled band in the t–J model (see e.g. [40]). $\mathbf{S}_i$ and $\mathbf{S}_j$ are the spin operators on lattice sites i and j and J is the exchange parameter. The summation is running over nearest neighbors.

Exchange interactions in this model can now be understood as follows. If every lattice site has one state per spin and is occupied by one electron (the exactly half filled band), than a virtual hopping process (one spin changes lattice site and forms an intermediate spin–zero–pair with its neighbor), is only allowed if neighboring spins have antiparallel

sign. The Pauli principle prohibits hopping for a ferromagnetic state. Although the energy cost of a $\uparrow\downarrow$ spin pair on one lattice site is U, the kinetic energy gain (from second–order perturbation theory) is $\sim \frac{t^2}{U}$, with the hopping parameter t and the on–site Coulomb term U (this is no other than the Hubbard–U). Usually U is of the range of 2–5 eV and t is of the order of 0.1 eV. Therefore the ordinary groundstate of the Heisenberg model is ferromagnetic. In several cases, for example the one dimensional Hubbard model, the kinetic energy gain due to the virtual admixture of doubly occupied sites outweights the cost of the on–site interaction and antiferromagnetic order is favorable [40]. Of course, as one can see from the Hamiltonian (3.48), again, the sign of J determines ferro- or antiferromagnetic order.

3.2.3 Superexchange

When working on transition metal oxides, it is of uttermost importance to familiarize oneself with the notion of superexchange. The concept was first brought up by Kramers in 1934 [41] and describes the magnetic coupling of two magnetic ions over the "bridge" of an unmagnetic one. This is the case for TMOs in the AFM II phase, where the biggest antiferromagnetic coupling of the transition metal ions is found between next nearest neighbors, with an oxygen ion in between. This was observed as early as 1949 by neutron diffraction for MnO [42]. In 1950 Anderson published a theory for superexchange and antiferromagnetism based on a spin–operator method [43], which was criticized by Slater for not dealing with non–orthogonality of overlapping wavefunctions [44]. The same criticism holds also for the approaches suggested by van Vleck and studied by several workers, namely an improved Heitler–London ansatz [45, 46]. In 1959, Anderson took a new viewpoint and tried to incorporate different suggested schemes as parts of the same physical mechanism [47]. In the present work the mathematical aspects of superexchange will be largely left aside, in favor of a phenomenological explanation which will follow ideas presented in [40]. For more detailed descriptions of the matter, one may consult the references given above, and the overview of several methods given in [48].

In a transition metal oxide, the electron hopping, that reduced the energy in the antiferromagnetic case in section 3.2.2, seems impossible, because the $3d$ orbitals of the transition metals, which carry the magnetic moments, are separated by a large Oxygen anion. Direct $3d$–$3d$ hopping seems very unlikely. To understand why the energy gain

of kinetic exchange can even be enhanced in such situations (some TMOs have quite high ordering temperatures) one can look at an idealized example.
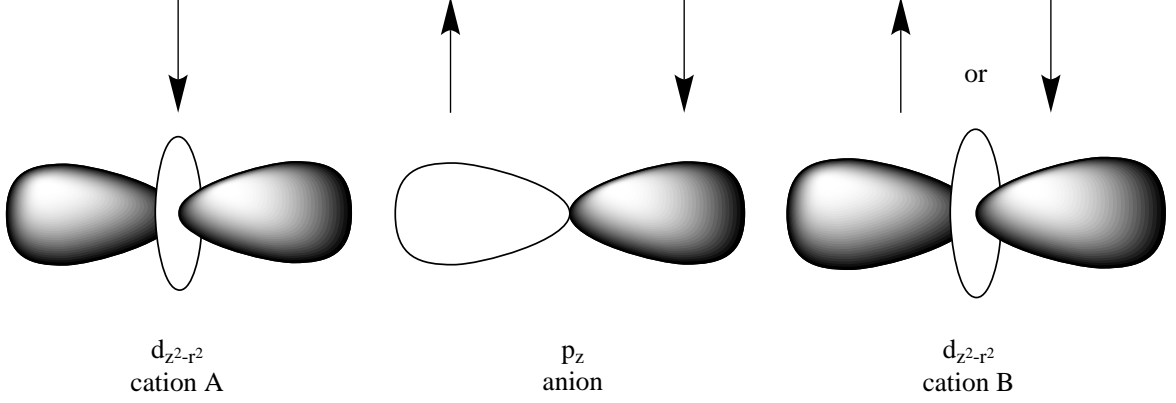

Figure 1: Superexchange of two cations via an intermediate anion.

In figure 1, two Ti^{3+} cations bond in a 180° angle with an O^{2-} anion in between. In this configuration, the cations have one electron each in their d shell, while the Oxygen $2p$ shell is completely filled. However, the $3d_{z^2-r^2}$ orbitals of the Ti ions hybridize with the O $2p_z$ orbital, and covalent mixing leads to a partially reoccupation of the d orbitals by the nominal p electrons, giving rise to fractional charges. But this rearrangement depends on the relative orientation of the cations d spins, thus the process transmits a d–d interaction. The following sketch of a deviation is based on the point of view of the p_z electrons for the two cases of cationic spin settings, $\downarrow\downarrow$ and $\downarrow\uparrow$. As seen in figure 1, the $\uparrow$-spin p electron can allways hop to the left and the resulting state will be a mix of p and d character.

$$| p_{z\uparrow} \rangle' \sim \frac{| p_{z\uparrow} \rangle + b\, | d_{A\uparrow} \rangle}{\sqrt{1 + b^2}} \tag{3.49}$$

The mixing amplitude b is derived from perturbation theory and it is assumed that $\epsilon_p < \epsilon_d$.

$$b \sim \frac{\langle p_z \,|\, \mathcal{H} \,|\, d_A \rangle}{\epsilon_p - \epsilon_d} \tag{3.50}$$

If now both d spins are $\downarrow$ (the ferromagnetic case), the same spin up electron can also travel to the cation on site B, while the Pauli principle prohibits hopping for the $p_{z\downarrow}$

electron. Thus the total energy of the two p electrons is approximately

$$
\begin{aligned}
E_{\downarrow\downarrow} &\sim \frac{1}{1 + 2b^2} \left(\langle p_{z\uparrow} | + b \langle d_{A\uparrow} | + b \langle d_{B\uparrow} | \right) \\
&\quad \langle p_{z\downarrow} | \mathcal{H} | p_{z\downarrow} \rangle \left(| p_{z\uparrow} \rangle + b | d_{A\uparrow} \rangle + b | d_{B\uparrow} \rangle \right) \\
&= 2\epsilon_p + \frac{2b^2}{1 + 2b^2} \left(\epsilon_p - \epsilon_d \right)
\end{aligned} \tag{3.51}
$$

For the antiferromagnetic case, where the d spin configuration is $\downarrow\uparrow$, the $p_{z\uparrow}$ electron can still hop to site A, but now the $p_{z\downarrow}$ electron can hop to site B. Its new state is thus

$$
| p_{z\downarrow} \rangle' \sim \frac{| p_{z\downarrow} \rangle + b | d_{B\downarrow} \rangle}{\sqrt{1 + b^2}} \quad . \tag{3.52}
$$

The total energy is evaluated at

$$
\begin{aligned}
E_{\downarrow\uparrow} &\sim {}'\langle p_{z\downarrow} | \, {}'\langle p_{z\uparrow} | \, \mathcal{H} | p_{z\uparrow} \rangle' | p_{z\downarrow} \rangle' \\
&= 2\epsilon_p + \frac{2b^2}{1 + b^2} \left(\epsilon_p - \epsilon_d \right)
\end{aligned} \tag{3.53}
$$

The splitting between this two configurations is the first effective exchange parameter $J_{\text{eff}}^{(1)}$.

$$
J_{\text{eff}}^{(1)} \sim E_{\downarrow\downarrow} - E_{\downarrow\uparrow} \sim 2b^4 \left(\epsilon_d - \epsilon_p \right) \tag{3.54}
$$

$J_{\text{eff}}^{(1)}$ is positive, which means that the $\downarrow\downarrow$ configuration costs more energy than the $\downarrow\uparrow$ configuration. The anion–mediated effective exchange, known as superexchange is thus antiferromagnetic.

In terms of perturbation theory, this is a fourth order process, with two electrons jumping away from the central anion, and two coming back. Another fourth order process is responsible for the second part of the interaction. Namely the changes introduced in the character of the d–states by the covalent mixing process. The new d-states are of $| d_A \rangle' \sim | d_A \rangle + b | p_z \rangle$ type, and even if the original d-orbitals were strictly non overlapping, an overlap of $\sim b^2(\epsilon_d - \epsilon_p)$ exists now on the anion site. This overlap is proportional to the hopping amplitude t_{AB}^* between the new d–states. It is now possible for a $\downarrow$–spin electron from cation A to jump to the anion site and then to site B, instantly followed by the $\uparrow$–spin electron from site B going the opposite way. This is

quite literally a spin exchange with the coupling

$$J_{\text{eff}}^{(2)} \sim 2\, b^4\, \frac{(\,\epsilon_d - \epsilon_p\,)^2}{U} \sim \frac{(t_{AB}^*)^2}{U} \quad . \tag{3.55}$$

The on site, intraatomic electron-electron repulsion U enters from the intermediate state, when both electrons are at the same cation site. The parameters derived in (3.54) and (3.55) now form the total superexchange coupling

$$J_{\text{eff}} = J_{\text{eff}}^{(1)} + J_{\text{eff}}^{(2)} \quad . \tag{3.56}$$

Thus the superexchange mechanism is quite analogous to the kinetic exchange discussed briefly in the last section.

It should be mentioned that the estimate given above is not a real calculation for a superexchange coupling constant. In reality higher lying orbitals have to be considered also, which leads to a dazzling number of intermediate states. Additional, the bond–angle plays a significant role and can even lead to a change in the sign of the interaction. The Goodenough-Kanamori rules, which were reformulated by Anderson, give guidelines for many cases and can be reviewed in e.g. [49].

4 Results

4.1 Atomic and Crystal Properties

In this section the chalcogen Oxygen, as well as the transition metals Scandium, Titanium, Vanadium, Chromium, Manganese, Iron, Cobalt and Nickel and their monoxides, are discussed briefly. An overview of the rocksalt crystal structure, which was used as a prototype model for all discussed TMOs, is also given.

4.1.1 Elements

- **Oxygen**

  Oxygen is the element with atomic number 8 and has the stable isotopes ^{16}O, ^{17}O and ^{18}O. Of those three, the configuration with 8 neutrons,^{16}O, is by far the most abundant (99.8%). The configuration of the eight electrons is 1s^2 2s^2 2p^4. At normal pressures and temperatures it forms the diatomic gas O_2. Due to its high electronegativity of 3.44 on the Pauling scale, Oxygen can build chemical bonds with nearly any other element.

- **Scandium**

  Scandium, with the chemical symbol Sc, has the atomic number 21 and exists naturally in a single isotope, ^{45}Sc. It therefor consists of 21 protons, 24 neutrons and 21 electrons. The electronic configuration is [Ar] 3d^1 4s^2. Scandium crystallizes in a hexagonal structure (hcp) with the lattice constant $a = 3.31$ Å and $c = 5.27$ Å [50]. The oxidation state is usually Sc^{3+} and it does not exist as a monoxide (ScO, or Scandium(II) oxide) but rather as Sc_2O_3 (Scandium(III) oxide).

- **Titanium**

  Titanium has five stable isotopes, ^{46}Ti to ^{50}Ti, with ^{48}Ti at 73.8% being the most abundant. This isotope has 22 protons, 26 neutrons and, in its neutral state, 22 electrons in the configuration [Ar] 3d^2 4s^2. The crystal structure is hexagonal with $a = 2.95$ Å and $c = 4.69$ Å [50]. The 4+ oxidation state dominates Titanium chemistry, but 3+, 2+ and 1+ states are also possible. Titanium monoxide is

non-stoichiometric in a range from $TiO_{0.7}$ to $TiO_{1.3}$ [51]. Pure TiO crystallizes in a defect rocksalt structure (fcc) with about 15% vacancies and $a = 4.18\,\text{Å}$ [50].

- **Vanadium**

  With 23 protons and electrons, Vanadium, with the symbol V, has one stable isotope, ^{51}V, with 28 neutrons. The electronic configuration of the neutral atom is [Ar] $3d^3$ $4s^2$. Vanadium has four common oxidation states, 5+, 4+, 3+ and 2+. Pure Vanadium adopts a body centered cubic crystal structure (bcc) with a lattice constant of $a = 3.02\,\text{Å}$ [50]. VO is a non-stoichiometric compound crystallizing in a rocksalt structure with $a = 4.06\,\text{Å}$ [50]. The composition varies between $V_{0.8}$ to $V_{1.3}$ [52].

- **Chromium**

  Three stable Chrome (Cr) isotopes exist, with 28, 29 or 30 neutrons. The most common of these is ^{52}Cr with 83.8% natural abundance. The element has 24 protons and electrons, the electron configuration being [Ar] $3d^5$ $4s^1$. At room temperature it forms an antiferromagnetic bcc crystal with the lattice constant $a = 2.88\,\text{Å}$ [50]. The principal oxidation states are 2+, 3+ and 6+, with Cr^{6+} being the most common. Its monoxide, CrO, crystallizes in the rocksalt structure [51].

- **Manganese**

  The element with the atomic number 25 and the symbol Mn exists in only one stable isotope, ^{55}Mn, with 30 neutrons. Its electron configuration is [Ar] $3d^5$ $4s^2$ and it crystallizes in the cubic, and quite unusual, α Manganese (A12) structure with a lattice constant of $a = 8.89\,\text{Å}$ [50]. Manganese is an antiferromagnet and its most common oxidation states include +2,+4 and +7. The TMO MnO forms in the rocksalt structure with $a = 4.44\,\text{Å}$ [50] and the composition can vary between MnO and $MnO_{1.045}$ [52].

- **Iron**

  The most common element on the planet, Iron, with the symbol Fe and the atomic number 26 has three stable isotopes with either 30, 31, or 32 neutrons. The configuration with 30 neutrons, ^{56}Fe, is the most common, with over 91.7% natural abundance. The 26 electrons arrange themselves in the configuration [Ar] $3d^6$ $4s^2$. Although Iron can have oxidation states ranging from -2 to +6, +2 and +3 are by far the most common. Fe crystallizes in the bcc structure with a lattice

constant of $a = 2.87\,\text{Å}$ [50] and is ferromagnetic. The fraction of iron in the non-stoichiometric compound Fe_xO varies typically between $Fe_{0.84}O$ and $Fe_{0.95}O$ [52]. Stoichiometric FeO has a lattice parameter of $a = 4.31\,\text{Å}$ [50].

- **Cobalt**

  The only stable Cobalt isotope, ^{59}Co has 28 protons and electrons and 32 neutrons. The electronic configuration is [Ar] $3d^7\ 4s^2$ and gives rise to the oxidation states -1,+1,+2,+3,+4 and +5, where +2 and +3 are the most common. Cobalt forms a ferromagnetic hcp unit cell with $a = 2.51\,\text{Å}$ and $c = 4.07\,\text{Å}$ [50]. CoO forms an antiferromagnetic (below $16\,^{\circ}$C [53]) rocksalt crystal with $a = 4.27\,\text{Å}$ [50].

- **Nickel**

  With an atomic number of 29, Nickel has five isotopes. ^{58}Ni, ^{60}Ni, ^{61}Ni, ^{62}Ni and ^{64}Ni, where ^{58}Ni, containing 30 neutrons is the most common with 86.1% natural abundance. Nickel crystallizes in a face centered cubic (fcc) structure with $a = 3.52\,\text{Å}$ [50] and is ferromagnetic. The electronic configuration is [Ar] $3d^9\ 4s^1$. The most common oxidation state is 2+, but 0, 1+, 3+ and even 4+ can occur. NiO, the only Nickel oxide, is non-stoichiometric and crystallizes in the rocksalt structure with $a = 4.17\,\text{Å}$ [50].

4.1.2 The Rocksalt Structure

The rocksalt structure (see figure 2), also known as halite structure, is, of course, called like that because of the NaCl prototype. It is basically a face centered cubic translational lattice system with two atoms in its unit cell. The primitive vectors of the fcc lattice are

$$\vec{A}_1 = \frac{1}{2}\,a \begin{pmatrix} 0 \\ 1 \\ 1 \end{pmatrix} \qquad \vec{A}_2 = \frac{1}{2}\,a \begin{pmatrix} 1 \\ 0 \\ 1 \end{pmatrix} \qquad \vec{A}_3 = \frac{1}{2}\,a \begin{pmatrix} 1 \\ 1 \\ 0 \end{pmatrix}$$

with a being the lattice parameter. The positions of the two ions are (were TM stands for transition metal):

$$\begin{aligned} \vec{B}_1 &= \vec{0} & \text{(TM)} \quad (4a) \\ \vec{B}_2 &= \frac{1}{2}\vec{A}_1 + \frac{1}{2}\vec{A}_2 + \frac{1}{2}\vec{A}_3 & \text{(O)} \quad (4b) \end{aligned}$$

The space group is Fm$\bar{3}$m with the number 225, the Pearson symbol is cF8 and the Strukturbericht designation is B1. If one wants to work with an antiferromagnetic system, one has to include four ions into the cell. Antiferromagnetism in rocksalt-type structures typically consists of ferromagnetic planes perpendicular to the 111 direction with alternating spin sign. This is known as the AFM II phase. The cell has than the new unit vectors

$$\vec{A}_1^{AF} = \frac{1}{2}\,a \begin{pmatrix} 2 \\ 1 \\ 1 \end{pmatrix} \qquad \vec{A}_2^{AF} = \frac{1}{2}\,a \begin{pmatrix} 1 \\ 2 \\ 1 \end{pmatrix} \qquad \vec{A}_3^{AF} = \frac{1}{2}\,a \begin{pmatrix} 1 \\ 1 \\ 2 \end{pmatrix}$$

and new ion positions.

$$\vec{B}_1 = \vec{0} \qquad \text{(TM)}$$

$$\vec{B}_2 = \frac{1}{2}\vec{A}_1 + \frac{1}{2}\vec{A}_2 + \frac{1}{2}\vec{A}_3 \qquad \text{(TM)}$$

$$\vec{B}_3 = \frac{1}{4}\vec{A}_1 + \frac{1}{4}\vec{A}_2 + \frac{1}{4}\vec{A}_3 \qquad \text{(O)}$$

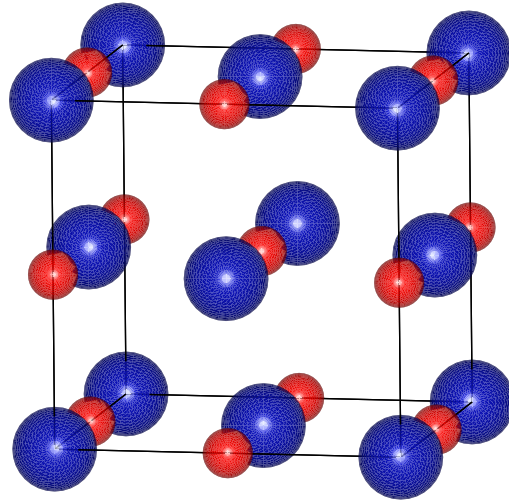$$\vec{B}_4 = \frac{3}{4}\vec{A}_1 + \frac{3}{4}\vec{A}_2 + \frac{3}{4}\vec{A}_3 \qquad \text{(O)}$$

Figure 2: Rocksalt structure

4.2 Bulk TMOs

The eight TMOs, ScO, TiO, VO, CrO, MnO, FeO, CoO and NiO, were analyzed using the HSE06 functional (see section 2.3) and the LDA+U method in the Dudarev flavor (see section 2.4). As a starting point PBE calculations (see section 2.2) were performed first.

After performing static antiferromagnetic HSE calculations (and ferromagnetic runs where the PBE calculations hinted in that direction), for several reasonable lattice parameters to find the equilibrium constant, an ideal parameter U was sought to mimic the HSE-obtained density of states (DOS). The LDA+U calculations were started at the lattice parameter found in the HSE runs, but the cell volume of the systems was allowed to relax, in order to obtain a groundstate. The cell shape, however, was kept constant and the ions were not allowed to deviate from their defined positions in the rocksalt structure. The U-optimization process was done as follows.

4.2.1 U and Δ Optimization Process

At first, the DOS was dissected into the three parts: Oxygen p-states, TM d_{eg}-states (containing the $d_{z^2-r^2}$ and the $d_{x^2-y^2}$ orbitals) and TM d_{t2g}-states (containing the d_{xy}, d_{yz} and d_{xz} orbitals). Each of these parts was than spilt at the Fermi-energy to form a "valance" and a "conduction" section, even when no bandgap was observed. For each of this six sections the first and second momentum of the function was evaluated, giving values corresponding to the peak position and the bandwidth. For conductors, all bandwidths and the peakpositions of both bands of a LDA+U run for a given U were compared directly with their HSE counterparts by calculating the quadratic deviation. For insulators and semiconductors, the peak positions of the conduction band were evaluated relatively to each other (e.g. TM d_{eg} $-$ O p) and the quadratic error was calculated for these differences. This was done to eliminate the influence of the bandgap, which is a major problem in TMOs, requiring sometimes enormous values of U, but can also be dealt with differently. As shown by Rödl et al. [54] an additional scissor shift Δ is easily incorporated into LDA+U (forming LDA+U+Δ) and allows to enlarge the bandgap by will. For this reason the magnitude of the gap was not considered in the U-optimization.

If one also includes the lattice constant, one counts now 13 conditions (6 bandwidths, 6 peak positions (of which 3 are relative in insulators), and the lattice parameter), which can be used to calculate the mean quadratic error of the LDA+U DOS in respect to the HSE DOS. To achieve a reasonable result, the quadratic deviations were scaled to be of comparable order of magnitude. The quadratic lattice constant errors were multiplied by a factor of 1000, whereas the quadratic bandwidth error was divided by 100 to get all to an order of magnitude 1.

It is not surprising, that one U in general can not optimize all of these parameters simultaneously and so, as can be seen in sections 4.2.3 to 4.2.10, different optimizations were carried out for each TMO.

4.2.2 PBE Calculations

All eight systems were calculated with the standard PBE-GGA functional in a nonmagnetic, a ferromagnetic and an antiferromagnetic setting. Each electronic system was relaxed at different lattice constants a, to determine the energy minimum. A full ionic relaxation was also performed to confirm these results.

	ScO	TiO	VO	CrO	MnO	FeO	CoO	NiO
NM - a	**4.48**	**4.29**	4.19	4.14	4.11	4.10	4.11	4.17
FM - a	4.48	4.29	4.26	**4.36**	4.45	**4.31**	4.25	4.20
AF - a	4.48	4.29	**4.32**	4.36	**4.44**	4.30	**4.22**	**4.19**
FM - μ	0	0	1.806	**3.719**	4.785	**4.001**	2.952	1.519
AF - μ	0	0	**2.365**	3.241	**4.316**	3.429	**2.400**	**1.305**
NM - E	**-17.090**	**-17.440**	-16.897	-15.849	-14.886	-13.823	-12.709	-11.471
FM - E	-17.090	-17.440	-16.933	**-16.727**	-16.477	**-15.030**	-13.078	-11.499
AF - E	-17.090	-17.440	**-17.157**	-16.601	**-16.628**	-15.004	**-13.231**	**-11.755**

Table 2: PBE lattice parameters (in Å), magnetic moments (in μ_b) and total energies (in eV) for nonmagnetic (NM), ferromagnetic (FM) and antiferromagnetic (AF) bulk TMOs. Values corresponding to lowest energies are printed bold.

As can be seen in table 2, ScO and TiO show no magnetism in the PBE approximation, but for all other TMOs, the magnetic ordered states have lower total energy than the nonmagnetic states. For VO, MnO, CoO and NiO, the antiferromagnetic state is the groundstate, while for CrO and FeO ferromagnetism leads to a lower energy solution.

4.2.3 ScO

Scandium monoxide has a single electron in the d-shell, so one would not expect much change by the LDA+U method in comparison to a PBE calculation. This is indeed true as shown in figure 3. However, this does not mean, that the GGA approximation works well in the case of ScO, but only states that electrons do not come close to each other in the d-orbital. The hybrid functional, using short range Fock exchange for all electrons, shifts the lower band, which has mainly Oxygen p character, down by about 2 eV in comparison to LDA+U. In figure 3, the HSE DOS is compared to three values of U, each one obtained by an optimization process. $U = 0.0$ is the best approximation if one wants to reproduce the HSE06 lattice constant. $U = 1.5$ optimizes the valence bandwidths, whereas $U = 2.2$ is best for the peak positions. $U = 2.2$ is also the value of choice if all parameters are considered in the optimization process. Lattice constants (a), magnetic moments per TM ion (μ) and fundamental bandgaps (Gap) are given in table 3 for all mentioned values of U. No other research on ScO in the rocksalt structure could be found, which is not too surprising, since it does not exist. Naturally, it is therefore not possible to provide any experimental data.

	a [Å]	μ [μ_b]	Gap [eV]
	Present work		
HSE06	4.440	0.001	0.0
U=0.0	4.478	0.000	0.0
U=1.5	4.517	0.000	0.0
U=2.2	4.536	0.000	0.0

Table 3: Data for bulk ScO

Summarizing, the LDA+U method does not provide a significant improvement over normal PBE calculations for ScO, because adding a larger and larger U only leads to an increasing lattice constant, which is already to big for $U = 0$. Figure 13 in section 4.2.11 shows the mean quadratic error dependent on U. While being rather large in comparison to the other tested systems, it does not vary much in the displayed region. The reason for the increase after the minimum at $U = 2.2$ is mainly the increasing lattice constant.
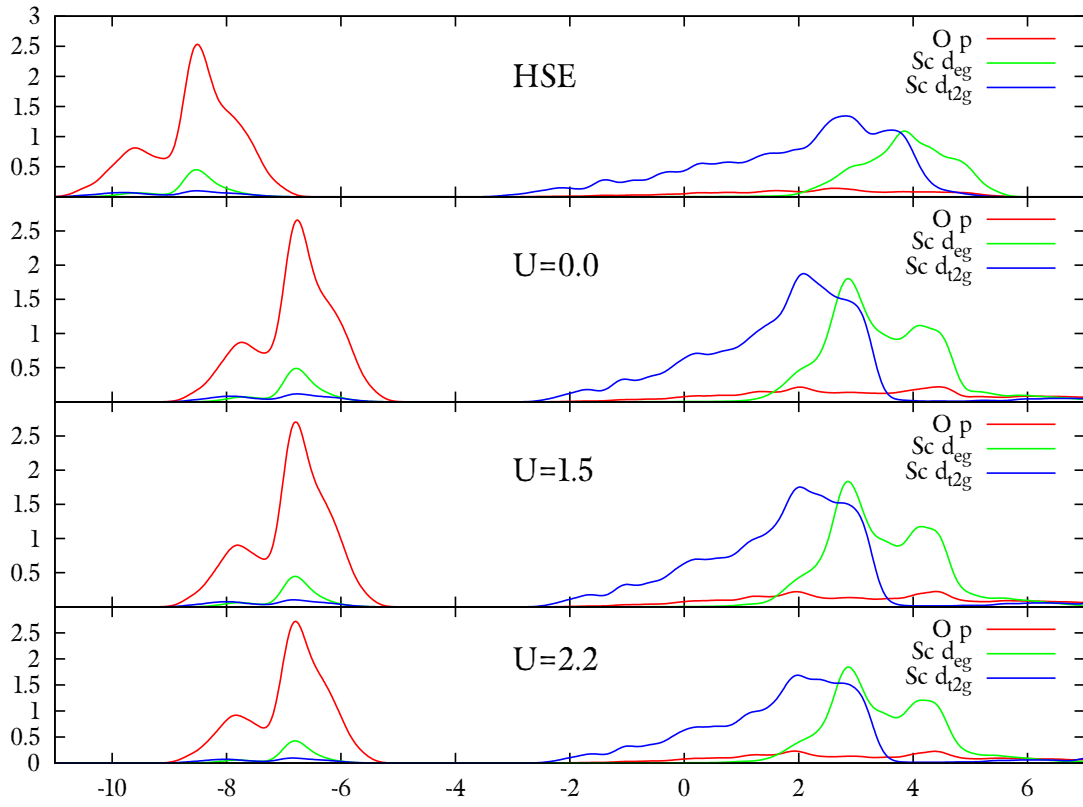
Figure 3: Bulk DOS of ScO (energy in eV)

4.2.4 TiO

If one considers the HSE06 and the LDA+U DOS graphs in figure 4, the difference in the width of the upper energy band is easily recognizable. The dip in the HSE DOS at the Fermi energy is also a pronounced feature, that is not seen (at least for lower values of U) in the LDA+U DOS. As observed for ScO, the lower LDA+U band is shifted upwards by about 1 eV in comparison to the HSE calculation. The whole DOS of TiO is very similar to the ScO DOS, for HSE as well as for very small U values, but in contrast to Scandium oxide, a profound change of the DOS is observed if the parameter U is increased. At short glance, $U = 2.6$ gives a rather good approximation of the HSE DOS, but the optimization process yields much smaller values. This might be the case because the two bands are not treated separately in the process, but the partition is made at the Fermi energy, in the middle of the upper band. For peak positions as well as for the optimization with respect to all parameters, the optimal U is found to be 0.6. If one optimizes for the lattice constant and the valence bandwidth, one gets U values of 1.0 and 0.0, respectively. However, the mean quadratic error does not change much at these low U values, as one can see in figure 13 in section 4.2.11.

	a [Å]	μ [μ_b]	Gap [eV]
		Present work	
HSE06	4.320	1.373	0.0
U=0.0	4.288	0.000	0.0
U=0.6	4.300	0.034	0.0
U=1.0	4.320	0.616	0.0
U=2.6	4.406	1.385	0.0

Table 4: Data for bulk TiO

Table 4 demonstrates that the magnetic moment is also just about right for $U = 2.6$. This, as well as the DOS graph, indicates that the optimization process, described in section 4.2.1, might not work properly in the case of TiO. As there were no publications to be found on stoichiometric TiO with no vacancies in the AFM II phase, it is unfortunately not possible to back up this idea with any data.
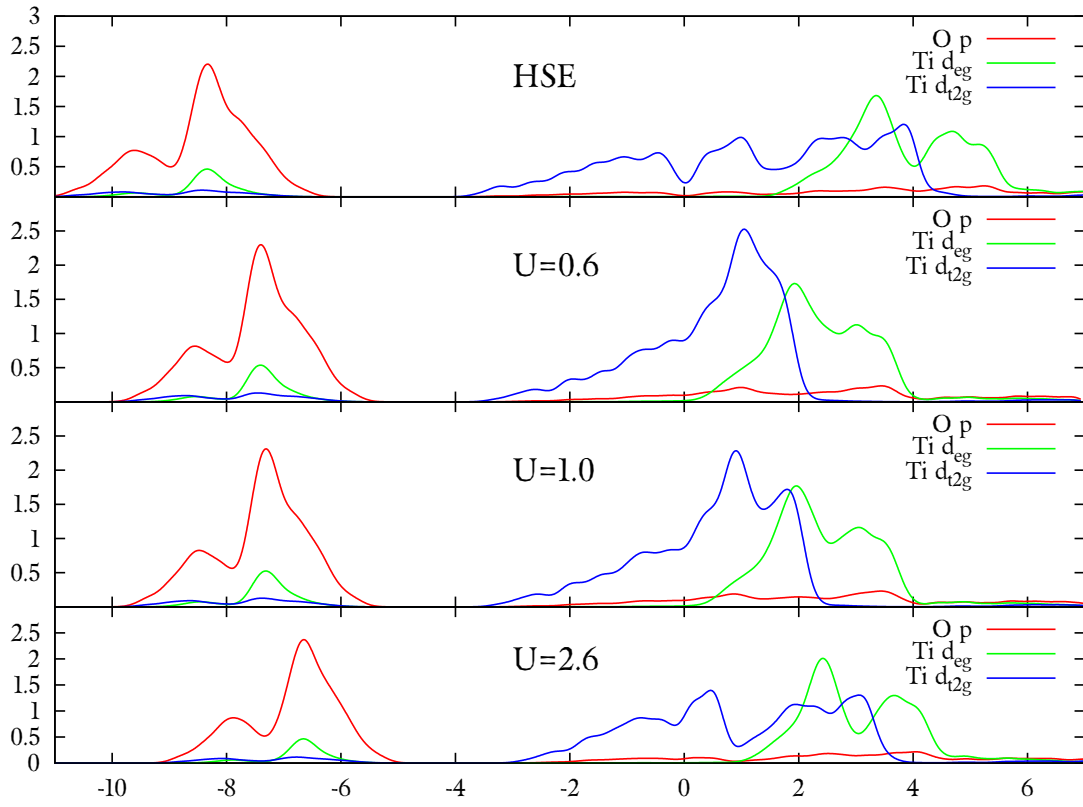
Figure 4: Bulk DOS of TiO (energy in eV)

4.2.5 VO

The HSE06 DOS of Vanadium oxide in the AFM II phase shows a semiconductor with three distinct bands. For very low values of U, the upper valence band in the LDA+U is joined with the conduction band at the Fermi energy, forming a metal. Other than the presence of the bandgap and the slightly broader bandwidth for the HSE calculations, the LDA+U approach works well in VO (see figure 5). The calculated optimal values of U are 0.2, 0.5, 0.8 and 1.3 for the lattice constant, valence bandwidth, peak positions and all parameters, respectively. The mean quadratic error for optimization with respect to all parameters is much lower than for ScO and TiO (see figure 13). With $U = 1.3$ and a $\Delta = 2.9$ a very good approximation to the HSE06 DOS is found with the LDA+U+Δ approach. While non spin polarized calculations predict VO to be a strongly correlated metal [55], Mackrodt et al. showed that introducing magnetism and exact exchange into the calculations produces a semiconductor, even down to 10% exact exchange contribution [56]. The group of Mackrodt found the AFM I phase, where the ferromagnetic planes of alternating spin are stacked along the (100), rather than the (111) direction, to be the groundstate of VO, but this phase is not discussed in this thesis. In table 5 the results from this work are compared with UHF (unrestricted Hartree-Fock) and B3LYP (a hybrid functional method) calculations for the AFM II phase by Mackrodt et al. [56].

As HSE06 uses 25% of exact exchange, the results should be comparable to the values given in table 5 for B3LYP (0.2). The lattice constant, as well as the magnetic moment and the bandgap are slightly smaller for HSE06, even though 5% more exact exchange was used. The bandgap scales linearly with higher percentages of HF-exchange, reaching over 14 eV for UHF. This is an order of magnitude larger as the gap predicted by HSE06, but as stoichiometric VO still features about 16% vacancies (see [55]), a comparison with experiments is not possible.

4.2.6 CrO

As the PBE groundstate of CrO was found to be ferromagnetic, rather than antiferromagnetic (see section 4.2.2), HSE06 calculations were carried out for both phases. The energy of the ferromagnetic phase remained lower than the antiferromagnetic one, but for the benefit of coherence, it was decided to fit the LDA+U model to the AFM II
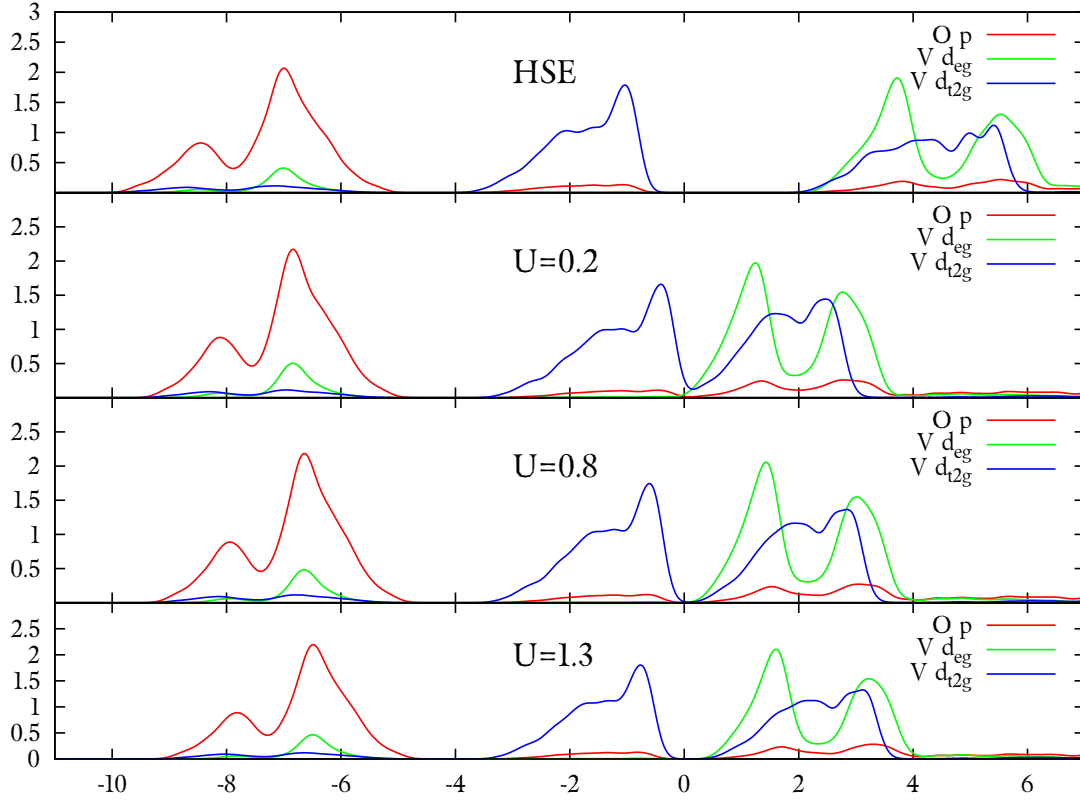
Figure 5: Bulk DOS of VO (energy in eV)

	a [Å]	μ [μ_b]	Gap [eV]
	Present work		
HSE06	4.330	2.599	2.896
U=0.2	4.327	2.390	0.0
U=0.5	4.339	2.442	0.0
U=0.8	4.349	2.480	0.0
U=1.3	4.363	2.527	0.0
	Previous calculations		
UHF[a]	4.4539	3.027	14.039
B3LYP (1.0)[a]	4.3528	2.983	14.142
B3LYP (0.8)[a]	4.3615	2.976	11.500
B3LYP (0.6)[a]	4.3737	2.965	8.896
B3LYP (0.4)[a]	4.3715	2.943	6.196
B3LYP (0.2)[a]	4.3824	2.891	3.239
B3LYP (0.1)[a]	4.3898	2.831	1.756

Table 5: Data for bulk VO; values in parentheses next to B3LYP denote fraction of exact exchange; [a]Reference [56]

phase.

Mainly, two things are happening to the PBE DOS (denoted by $U = 0.0$ in figure 6) of CrO if one quarter of exact exchange is introduced by the HSE06 functional: First, the d_{t2g} states are split at the Fermi energy, and the lower energy part is shifted downwards by about 1.5 eV, while the upper part is shifted to about 2 eV higher energies. Second, the d_{eg} states are split into three parts (all containing $d_{z^2-r^2}$ as well as $d_{x^2-y^2}$ orbitals), one of which stays at the Fermi level, while the two others are shifted upwards and downwards, respectively. While the behavior of the d_{t2g} states is mimicked well by the LDA+U approach, the d_{eg} splitting at the Fermi level does not occur. This results in a much higher density of states at the Fermi energy for LDA+U as for HSE. Other than that, bandwidths and peak positions are quite well reproduced and the overall error is rather small (see figure 13). The ideal values of U are found to be: 0.0 for the valence bandwidth, 1.2 for the lattice constant, 2.9 overall and 4.6 for the peak positions. Lattice constants, magnetic moments and bandgaps are found in table 6. No data from experiments or other calculations could be obtained.
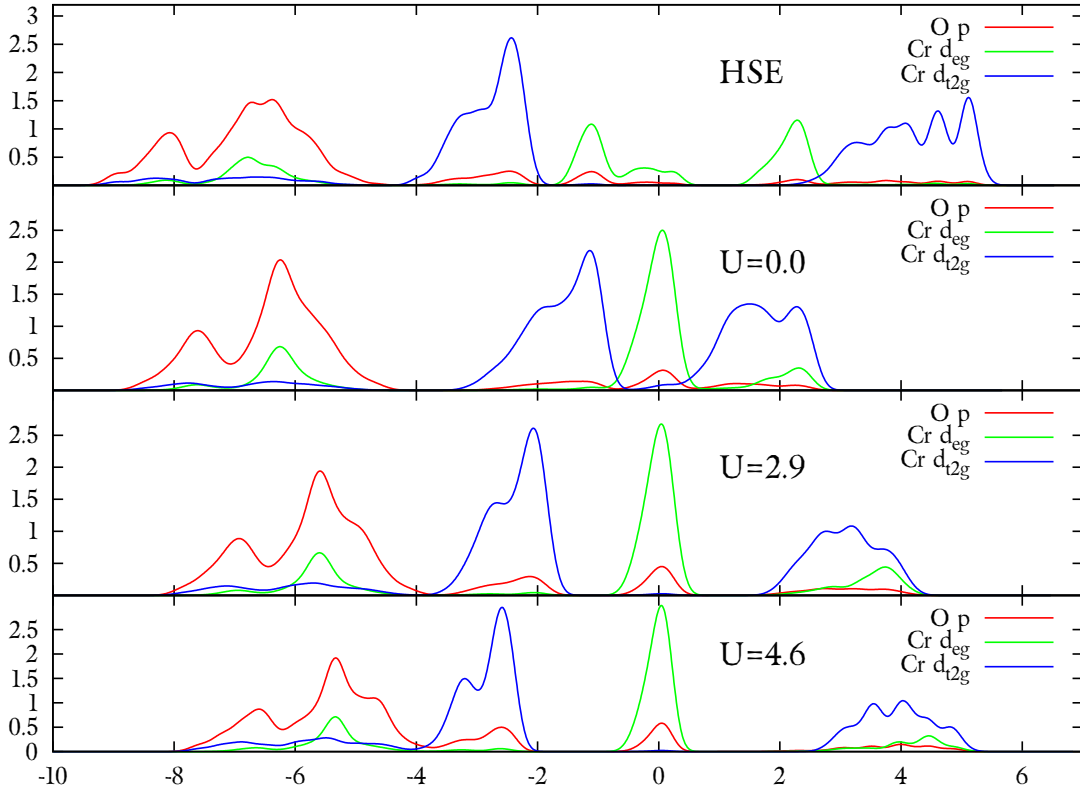
Figure 6: Bulk DOS of CrO (energy in eV)

	a [Å]	μ [μ_b]	Gap [eV]
		Present work	
HSE06	4.390	3.674	0.0
U=0.0	4.357	3.424	0.0
U=1.2	4.390	3.601	0.0
U=2.9	4.431	3.771	0.0
U=4.6	4.459	3.896	0.0

Table 6: Data for bulk CrO

4.2.7 MnO

In the HSE calculation of this work MnO, in the AFM II phase, has a substantial bandgap of 2.98 eV. While a gap is reproducible with LDA+U, it is significantly smaller for reasonable values of U, that do not distort the rest of the DOS too much. As figure 7 shows, $U = 2.3$, the optimized value for the peak positions, mimics the valence DOS very well. If the valence bandwidths are the focus of interest, an even lower value of U, 1.4, is the appropriate one, and $U = 0.8$ minimizes the error in the lattice constant. The broadening of the conduction Mn d_{t2g} states with rising values of U, leads to an much larger optimal U of 3.8 if all parameters (peak positions, bandwidths and lattice constant) are considered. This value leads to a sizable gap, so only a rather small Δ of 1.3 is needed to reach the HSE value. Rödl et al. [54] reported a smaller value of U, combined with a larger Δ, of 2.0 and 3.0 respectively.

The weighted mean quadratic error for $U = 3.8$ with respect to the HSE06 calculation is 1.3. Figure 13 shows the U-dependence of the error. In table 7 calculated data from this thesis is compared to other calculations and experiments.
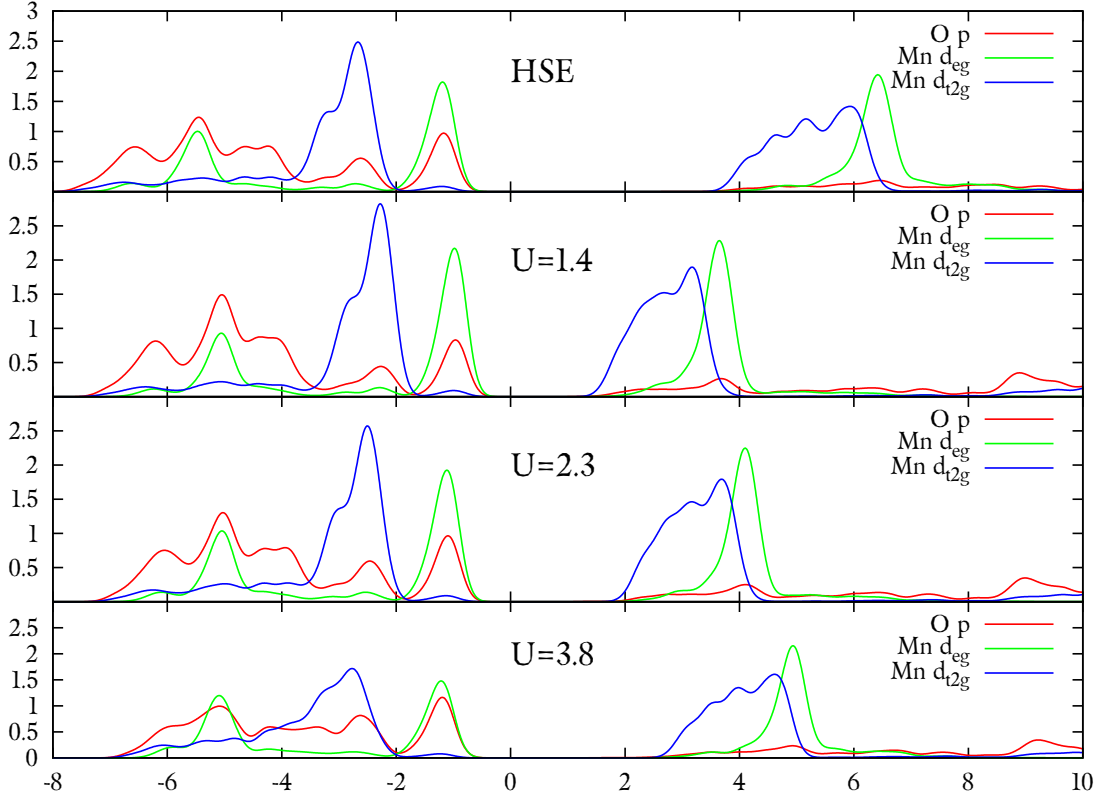
Figure 7: Bulk DOS of MnO (energy in eV)

The Abbreviations used in table 7 (and following tables) read as follows. EXX: exact exchange. FPLO: full potential local orbital method with Perdew-Wang (1992) exchange-correlation functional. Gaussian: Gaussian local orbital code, Slater exchange ($\alpha = 2/3$) and Vosko-Wilk-Nusair correlation. PW-US-PP: plane-wave basis using ultrasoft pseudopotentials, with the Perdew-Zunger exchange-correlation functional. LMTO-ASA: linear muffin-tin orbital code in the atomic sphere approximation, using the Perdew-Zunger exchange-correlation functional. XD: x-ray diffraction. XPS: x-ray photoemission spectroscopy. BIS: bremsstrahlung-isochromat spectroscopy.

In a nutshell, the most simple transition metal oxide (with its exactly half filled d-shell), can be very well described with the LDA+U method. A gap in the right order of magnitude is opened by $U = 3.8$ and can be easily enlarged to the HSE result by adding a Δ of 1.3.

54

	a [Å]	μ [μ_b]	Gap [eV]
	Present work		
HSE06	4.450	4.524	2.98
U=0.8	4.452	4.392	0.054
U=1.4	4.458	4.439	1.272
U=2.3	4.469	4.500	1.460
U=3.8	4.485	4.585	1.724
	Previous calculations		
HSE03[a]	-	4.50	2.60
HSE03+G_0W_0[a]	-	-	3.40
GGA[a]	-	4.30	0.70
GGA+U[a]	-	4.50	-
EXX[b]	4.445	4.81	3.85
FPLO[c]	4.317	4.52	0.72
Gaussian[c]	4.317	4.53	1.13
PW-US-PP[c]	4.272	4.42	0.92
LMTO-ASA[c]	4.317	4.42	1.04
PBE[d]	4.450	4.26	0.90
LDA+U[d]	4.400	4.50	1.90
B3PW91[d]	4.460	4.38	1.30
PBE0[d]	4.510	4.40	1.30
	Experiments		
[e]	4.45	-	-
neutron diffraction[f]	-	5	-
γ-ray diffraction[g]	-	4.54(5)	-
neutron diffraction[h]	4.432*	4.58	-
XD, XPS, BIS[i]	4.4415	-	3.9

Table 7: Data for bulk MnO; *distorted rocksalt (=rhombohedral) structure ($\alpha >$ 90°); [a]Reference [54], [b]Reference [57], [c]Reference [58], [d]Reference [59], [e]Reference [50], [f]Reference [60], [g]Reference [61], [h]Reference [62], [i]Reference [63]

4.2.8 FeO

As seen in table 2 in section 4.2.2, the PBE groundstate of FeO is ferromagnetic. When treated with the HSE06 functional, this is no longer true, and the AFM II phase has lower energy. Also, HSE opens a bandgap of 2.23 eV. This gap was found to be irreproducible by means of LDA+U alone, even if the structure was totally relaxed and lattice distortions were allowed. As one can see in figure 8, the Fe d_{t2g} orbital presents itself with one single- and one double-peak around the Fermi energy. For HSE, the double-peak (an overlap of two peaks), is located in the conduction band and the single one forms the top of the valence band. In case of LDA+U, the situation is very different. The three peaks are split at another point, so that the double-peak is located at a lower energy compared to the single one. The double-peak then sits unmoving at the Fermi energy, while the single-peak is shifted upwards in energy with increasing U. Thus, in contrast to MnO, it is not possible to describe FeO well with LDA+U. However, if one is willing to introduce another fit parameter, the scissor shift Δ, into the model, good agreements can be achieved. To fit the (relative) peak positions, the parameter $U = 3.2$ was calculated in this thesis. Optimization with respect to valence bandwidth and lattice constant yields $U = 3.5$ and $U = 2.9$, respectively. An optimization of all parameters leads to a U of 3.8, the same as for MnO. The corresponding value for Δ is 2.2. The parameters found in [54] are $U = 3.0$ and $\Delta = 1.5$. Data is shown in table 8.

4.2.9 CoO

According to [65] CoO at room temperature is cubic and paramagnetic with $a = 4.2614$ Å. The transition to the antiferromagnetic ordered phase is accompanied by a change of lattice symmetry to a monoclinic structure. At 10 Kelvin the lattice constants are $a = 5.1819$ Å, $b = 3.0176$ Å and $c = 3.0186$ Å. For reason of simplicity the cubic rocksalt structure was used for the AFM II phase as well in this work. The HSE06 calculation then yields a gap of 3.5. As can be seen in figure 9, The LDA+U approach opens a bandgap if $U \geq 2.0$. To minimize the errors in the peak position a U value of 1.5 was calculated, which is also the optimum if one includes all parameters. While the parameters $U = 3.0$ and $\Delta = 2.5$ are given by [54], $U = 1.5$ and $\Delta = 3.5$ are proposed here. For the valence bandwidth one obtains $U = 2.2$, and for the lattice constant one seems to have a choice between $U = 1.0$ and $U = 4.2$. This is quite astonishing, because usually a larger U leads to a larger lattice constant.
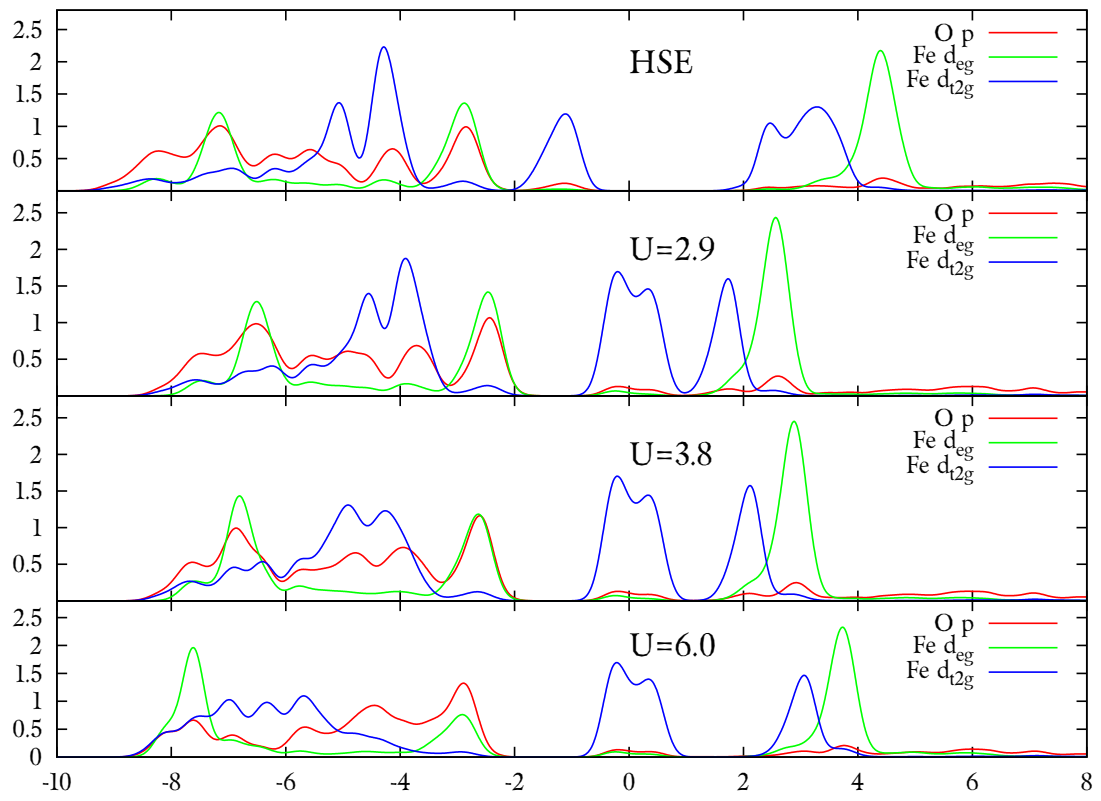
Figure 8: Bulk DOS of FeO (energy in eV)

	a [Å]	μ [μ_b]	Gap [eV]
Present work			
HSE06	4.330	3.630	2.23
U=2.9	4.330	3.648	0.0
U=3.2	4.331	3.665	0.0
U=3.5	4.332	3.682	0.0
U=3.8	4.334	3.698	0.0
Previous calculations			
HSE03[a]	-	3.40	2.1
HSE03+G_0W_0[a]	-	-	2.2
GGA[a]	-	3.40	0.0
GGA+U[a]	-	3.60	-
EXX[b]	4.334	3.85	1.66
PBE[c]	4.300	3.49	0.0
LDA+U[c]	4.280	4.23	0.0
B3PW91[c]	4.350	4.15	1.3
PBE0[c]	4.400	4.30	1.2
Experiments			
[d]	4.31	-	-
neutron diffraction[e]	-	3.32	-
[f]	-	-	2.4

Table 8: Data for bulk FeO; [a]Reference [54], [b]Reference [57], [c]Reference [59], [d]Reference [50], [e]Reference [60], [f]Reference [64]
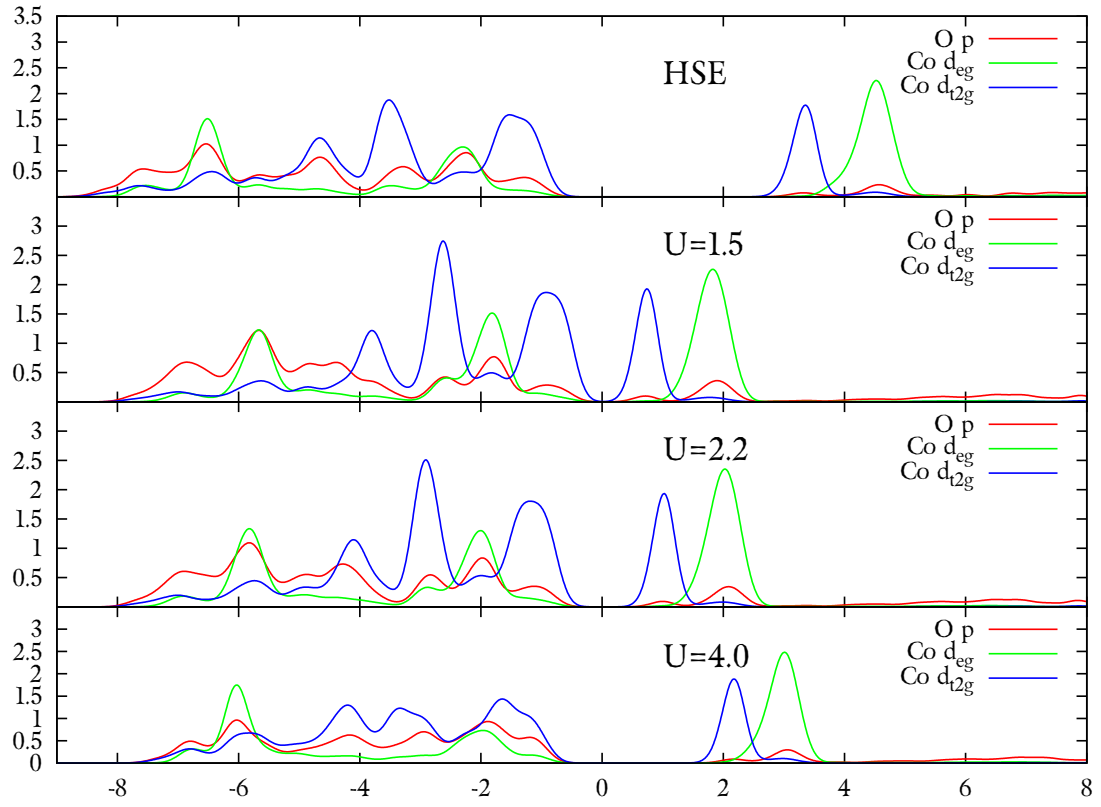
Figure 9: Bulk DOS of CoO (energy in eV)

This behavior is connected to a sudden change in the DOS, the energy and the lattice constant, between $U = 4.1$ and $U = 4.2$, as can be seen in figure 10. It corresponds to an insulator–conductor transition with an energy difference of about $+1.5$ eV.
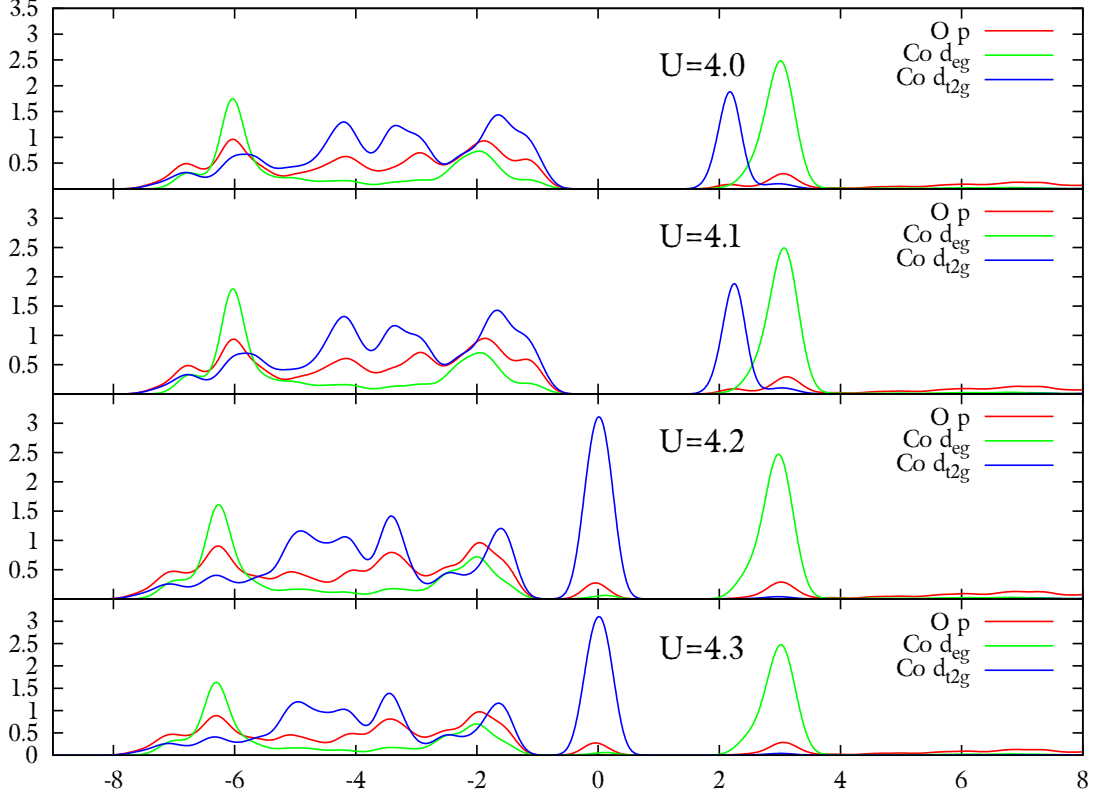
Figure 10: Bulk DOS of CoO (energy in eV)

This phase transition only occurs if one allows only a relaxation of the structures volume, but not its cell shape or the ion positions. If these degrees of freedom are turned on, the continuous behavior returns, as can be seen in figure 11. Also, if the wavefunctions of the fully relaxed run are used as a starting point for a volume relaxation, the insulator–conductor transition does not occur. The same is true if the symmetry is broken by shifting one of the Co ions very slightly ($< 1\%$) from its ideal position. The perfect agreement of the LDA$+U$ lattice constant with its HSE counterpart at $U = 4.2$ (and slightly higher values) should therefore be ignored in the context of this work, as it is only valid in context of the phase transition. Giving that the structure of CoO in the AFM II phase is really monoclinic and not cubic, it is not surprising that unforseen results can occur if the crystal is forced into a "wrong" shape. Astonishing, however, is the very sudden appearance of the conduction state, by changing U by just 0.1 eV. The above mentioned phase transition serves as a good reminder for being attentive while

calculating magnetically ordered structures. Symmetries or the breaking of symmetries might be very important to change magnetic ordering or conductivity. Table 9 shows a collection of data from this work, previous studies and experiments for CoO.
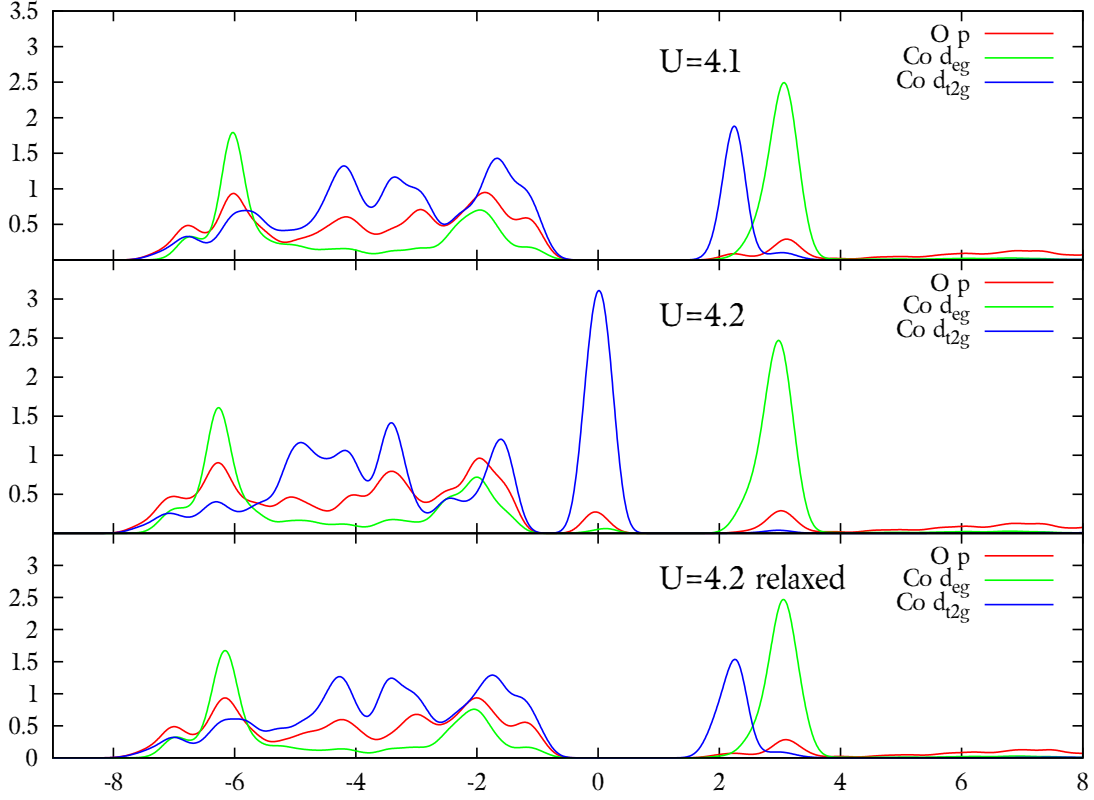
Figure 11: Bulk DOS of CoO (energy in eV)

4.2.10 NiO

If Nickel oxide in the AFM II phase is treated with the HSE06 functional it yields a bandgap of 4.4 eV. Other groups ([54, 59]) report the opening of a gap of about 0.5 eV for GGA calculations, which cannot be confirmed by this work due to the large DOS smearing used. In figure 12, the PBE result can be seen in the part marked with $U = 0.0$. While the DOS graph drops significantly at the Fermi energy, fractional occupation numbers show that no gap is formed. Nevertheless a sizable gap of 1.251 is observed at a quite low U value of 1.0. Optimization for peak positions, lattice constant, valence bandwidths and all parameters combined result in U values of 3.5, 0.0, 3.5 and 5.3, respectively. A U of 5.3 opens a bandgap of 3.1, so a Δ of 1.3 must be used to

	a [Å]	μ [μ_b]	Gap [eV]
Present work			
HSE06	4.260	2.668	3.535
U=1.0	4.260	2.493	0.0
U=1.5	4.263	2.531	0.0
U=2.2	4.275	2.581	1.345
U=4.0	4.286	2.680	2.390
Previous calculations			
HSE03[a]	-	2.40	3.20
HSE03+G_0W_0[a]	-	-	3.40
GGA[a]	-	2.40	0.00
GGA+U[a]	-	2.60	-
EXX[b]	4.254	2.88	2.62
PBE[c]	4.240	2.60	0.00
LDA+U[c]	4.200	3.48	2.70
B3PW91[c]	4.280	3.23	2.00
PBE0[c]	4.320	4.14	2.10
Experiments			
[d]	4.27	-	-
neutron diffraction[e]	-	3.8	-
x-ray diffraction[f]	4.267	3.98	-

Table 9: Data for bulk CoO; [a]Reference [54], [b]Reference [57], [c]Reference [59], [d]Reference [50], [e]Reference [60], [f]Reference [65]

mimic the HSE behavior. Rödl et al. report values of $U = 3.0$ and $\Delta = 2.0$ [54]. More data for NiO can be found in table 10.
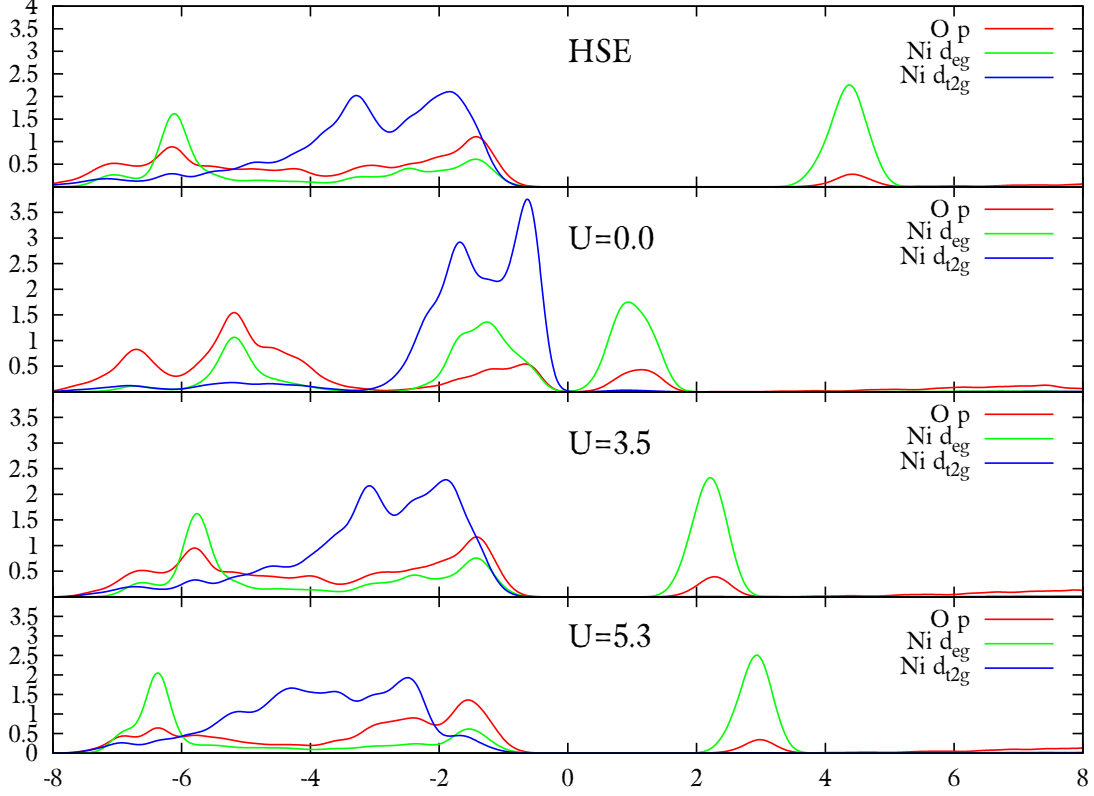
Figure 12: Bulk DOS of NiO (energy in eV)

4.2.11 Bulk TMO Summary

In this short summary, the values of U and Δ, as found by optimizing with respect to all parameters, are given for each transition metal oxide and compared to the previous calculation by Rödl et al. [54] (see table 11). The U values given in reference [54], are, with the exception of CoO, lower than the parameters calculated in the present work. If one optimizes with respect to the peak positions, the values match quite well, with CoO being the exception again. Summing up, it is not possible to mimic all aspects of the HSE06 DOS with a single U in the case of the bulk TMOs considered in this work. If the system is too large to allow an HSE calculation, one has to decide which feature is most important, or accept an equal deviation for all facets by choosing the parameters given in table 11. Figure 13 shows the U dependence of the mean quadratic DOS error for each TMO.

	a [Å]	μ [μ_b]	Gap [eV]
Present work			
HSE06	4.190	1.659	4.416
U=0.0	4.190	1.299	0.0
U=3.5	4.194	1.596	2.378
U=5.3	4.196	1.689	3.084
Previous calculations			
HSE03[a]	-	1.60	4.1
HSE03+G_0W_0[a]	-	-	4.7
GGA[a]	-	1.30	0.6
GGA+U[a]	-	1.50	-
EXX[b]	4.171	1.89	4.1
PBE[c]	4.200	1.21	0.4
LDA+U[c]	4.120	1.72	3.2
B3PW91[c]	4.210	1.70	2.8
PBE0[c]	4.240	1.73	2.8
Experiments			
[d]	4.17	-	-
neutron diffraction[e]	4.170	1.90	-
XPS, BIS[f]	-	-	4.0
Photoemission[g]	-	-	4.3

Table 10: Data for bulk NiO; [a]Reference [54], [b]Reference [57], [c]Reference [59], [d]Reference [50], [e]Reference [62], [f]Reference [66], [g]Reference [67]

	ScO	TiO	VO	CrO	MnO	FeO	CoO	NiO
Present work								
U [eV]	2.2	0.6	1.3	2.9	3.8	3.8	1.5	5.3
Δ [eV]	0.0	0.0	2.9	0.0	1.3	2.2	3.5	1.3
Reference [54]								
U [eV]	-	-	-	-	2.0	3.0	3.0	3.0
Δ [eV]	-	-	-	-	3.0	1.5	2.5	2.0

Table 11: Parameters U and Δ for bulk TMOs
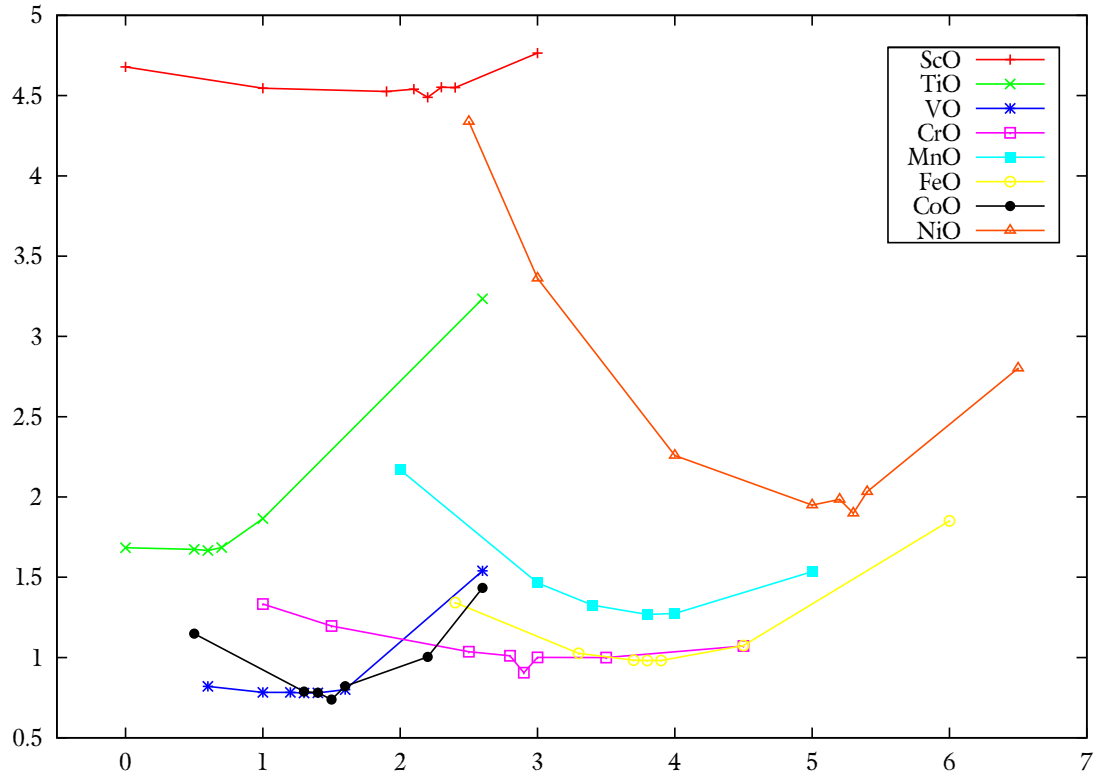
Figure 13: U dependent mean quadratic DOS error between HSE06 and LDA+U for bulk TMOs. (U in eV on the x-axis, error in arbitrary units on the y-axis)

4.3 Monolayer

All eight $3d$ transition metal monoxides were also analyzed in the form of a monolayer. The layer was "cut" along the (100) direction of the cell, so that transition metal ions and oxygen ions form a checkerboard pattern in the x-y-plain. A distance of three lattice constants was left between repeating monolayers, which computes to more than 12 Å in any case. Thus, the primitive vectors are

$$\vec{A}_1 = a \begin{pmatrix} 1 \\ 0 \\ 0 \end{pmatrix} \qquad \vec{A}_2 = a \begin{pmatrix} 0 \\ 1 \\ 0 \end{pmatrix} \qquad \vec{A}_3 = a \begin{pmatrix} 0 \\ 0 \\ 3 \end{pmatrix}$$

with a being the lattice parameter. The four ions necessary for an antiferromagnetic solution are then positioned at

$$\begin{aligned} \vec{B}_1 &= & 0 & \quad \text{(TM)} \\ \vec{B}_2 &= \frac{1}{2}\vec{A}_1 + \frac{1}{2}\vec{A}_2 & & \quad \text{(TM)} \\ \vec{B}_3 &= & \frac{1}{2}\vec{A}_1 & \quad \text{(O)} \\ \vec{B}_4 &= & \frac{1}{2}\vec{A}_2 & \quad \text{(O)} \end{aligned}$$

were TM denotes a transition metal ion and O an Oxygen site. By assigning the TM at position $\vec{B}_1$ spin "up" and the TM at $\vec{B}_2$ spin "down", the coupling between nearest TM neighbors $(d = \frac{\sqrt{2}}{2} a)$ is antiferromagnetic. Therfore the dominant process for magnetic coupling is direct exchange rather than superexchange, as in the bulk configuration (see section 3.2.3).

The monolayer was used to simulate an "ideal surface", and the idea of the effort was to provide values of U, that may approximate the parameter in surface layers of a real slab. By comparing bulk and monolayer values, one may find at least starting numbers for more complex surface calculations. The U optimization process was in essence the same as for the bulk calculations (see section 4.2.1), but the lattice constant was omitted as a parameter. All calculations were done at the bulk HSE lattice constants of the respective TMOs and no relaxations were performed to simulate the stress on a real surface layer, which also has to retain the bulk lattice constant. DOS graphs and

further information on the monolayer calculations, from ScO too CoO, can be reviewed in sections 4.3.1 to 4.3.7. For NiO, the HSE calculation gave unphysical results, and no comparison to LDA+U was performed. There were no previous calculations to be found for TMO monolayers, so no references are given.

4.3.1 ScO

In contrast to bulk ScO, the monolayer converges to an antiferromagnetic solution for both HSE06 and LDA+U, if one initializes antiparallel magnetic moments. Even for $U = 0$, which is equivalent to PBE, the magnetic moments reach half of the HSE value. As shown in figure 14, increasing U does not help to push down the Oxygen p–states to the appropriate HSE position. The most noticeable change in the LDA+U DOS with increasing U is the splitting of the d_{t2g} and d_{eg} states, which first approaches the HSE situation and then even leads to a metal–insulator transition. At $U = 7.0$ a sizable gap of 1.6 eV has formed. The optimal U values found were 5.2 for the peak positions and for the overall optimization and 6.1 for the valence bandwidth. Data is shown in table 12. All things considered, one has to conclude that the approximation of the HSE06 DOS with the LDA+U method works quite well in the case of an ScO monolayer. This result is somewhat different from the bulk situation, were the variation of U did not change a lot in the DOS. The quadratic deviation from the HSE DOS for different values of U can be observed in figure 21 in section 4.3.8.

	μ [μ_b]	Gap [eV]
HSE06	0.476	0.0
U=0.0	0.225	0.0
U=5.2	0.602	0.0
U=6.1	0.629	0.020
U=7.0	0.659	1.603

Table 12: Data for ScO (100) monolayer

4.3.2 TiO

As in the bulk HSE calculation, the monolayer HSE06 DOS of Titanium oxide is quite low at the Fermi energy (see figure 15). PBE does not show this behavior but
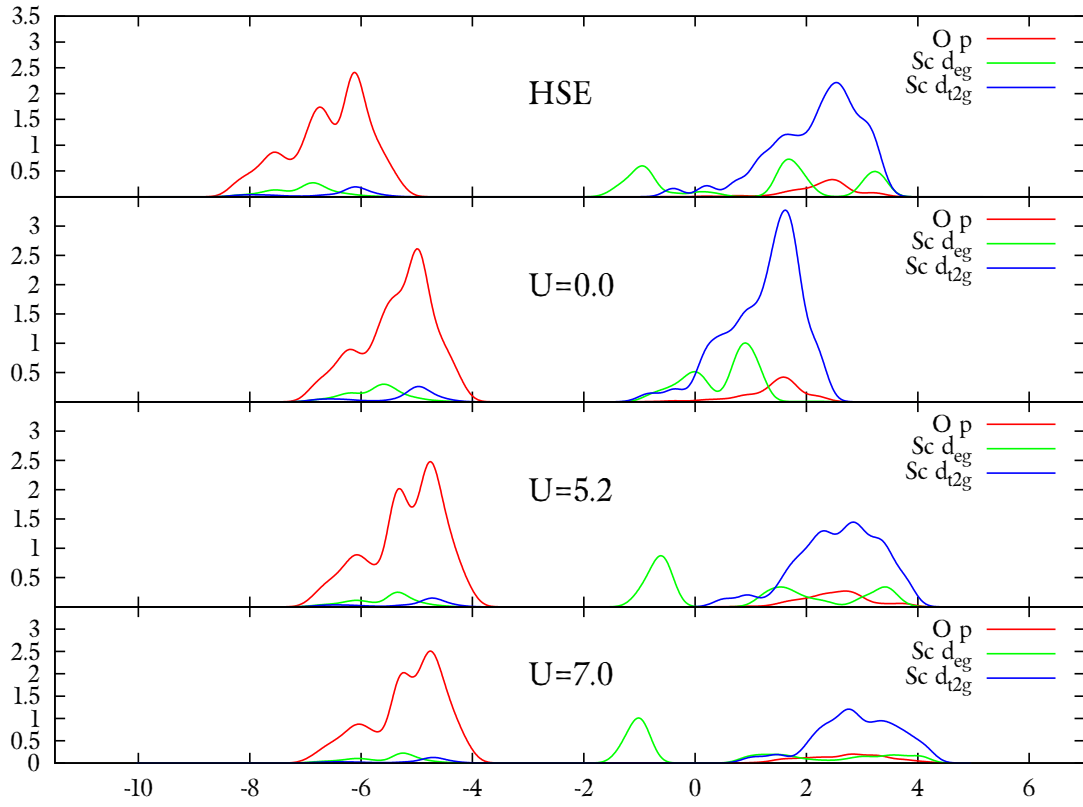
Figure 14: DOS of ScO (100) monolayer (energy in eV)

it is reproducible with LDA+U. However, it is difficult to broaden the conduction band to its HSE value of about 8 eV, because the DOS at the Fermi level decreases with increasing U, till a gap is opened at about $U = 6.0$. As it was the case for the ScO monolayer, the Oxygen p–band is located about two eV lower than its PBE counterpart, and increasing U does not push this band to lower energies, but shifts it nearer to the Fermi level. The optimal parameters found for TiO are very similar for every optimization, yielding $U = 2.5$ for the valence bandwidth and $U = 2.6$ for the peak positions and the overall optimization. It is definitely a plus, that it is possible to mimic every aspect of the HSE06 DOS with the essential same value of U, but the overall quadratic mean error is quite high in comparison to the other TMOs, as one can see in figure 21. Data for TiO is found in table 13.
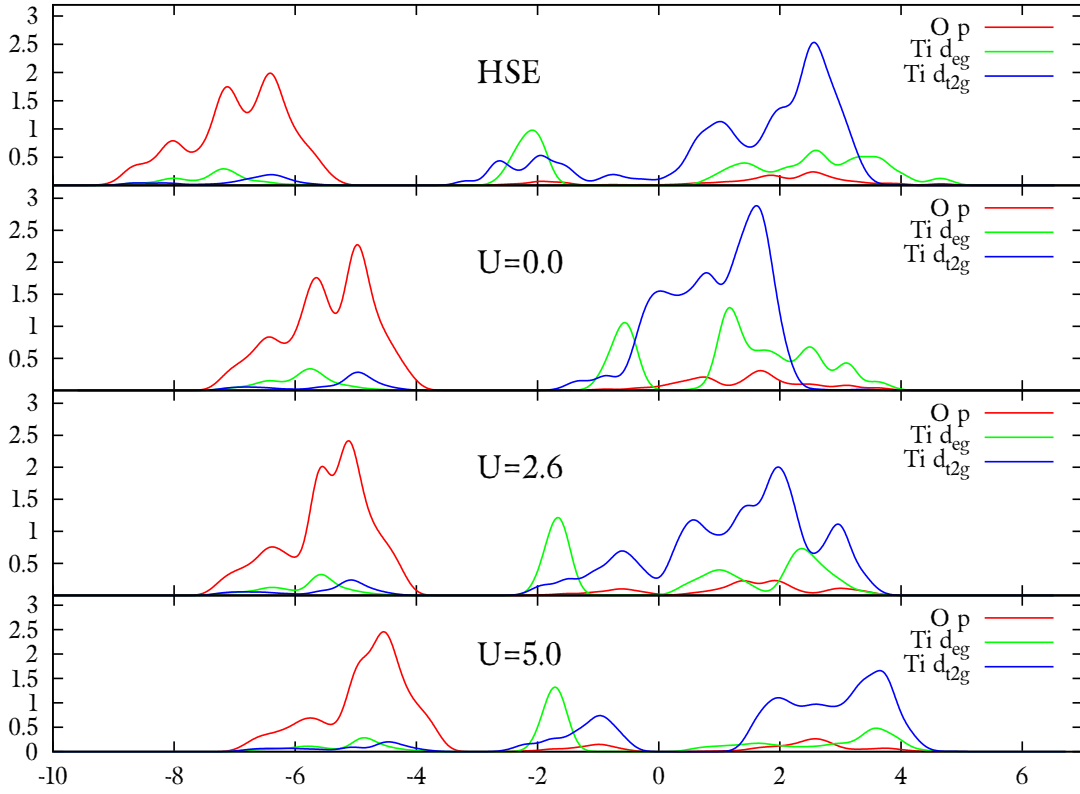
Figure 15: DOS of TiO (100) monolayer (energy in eV)

4.3.3 VO

Unlike in bulk, the HSE06 calculation for the VO monolayer yields a metallic DOS with a broad d_{t2g} peak at the Fermi level (see figure 16). Increasing U does not change

	$\mu\ [\mu_b]$	Gap [eV]
HSE06	1.438	0.0
U=0.0	1.123	0.0
U=2.6	1.503	0.0
U=5.0	1.627	0.0

Table 13: Data for TiO (100) monolayer

the occupation numbers of the orbitals, but shifts all d states away from the central d_{t2g} peak. The U values found in the optimization process for the peak positions and for all parameters are quite close, with $U = 4.9$ and $U = 5.2$, respectively. However, in contrast to TiO, the ideal parameter for the valence bandwidth, at $U = 0.0$, is very different. As there is no gap for any calculation no parameter Δ is needed. The mean quadratic error (figure 21) is quite low and features a broad and not very pronounced minimum. All things considered, the HSE06 calculation of the VO monolayer is nicely reproducible with the LDA+U method. Magnetic moments and fundamental bandgaps are given in table 14.

	$\mu\ [\mu_b]$	Gap [eV]
HSE06	2.594	0.0
U=0.0	2.406	0.0
U=2.4	2.583	0.0
U=4.9	2.690	0.0
U=5.2	2.702	0.0

Table 14: Data for VO (100) monolayer

4.3.4 CrO

For CrO the calculated values for U depend strongly on the parameters which were chosen for the optimization. $U = 0.0$ is best for the valence bandwidth, $U = 1.7$ is for the peak positions and $U = 4.5$ is ideal for all parameters combined. In contrast to VO however, a gap is opening at reasonable low U values. Still, to reach the same gap size, a Δ of 0.7 eV is required for $U = 4.5$. While the valence DOS of the CrO monolayer is very well reproduced by the LDA+U method (see figure 17), the prominent peak of the conducting d_{eg} states is missing. For $U > 3.0$, also the d_{t2g} peak is starting to
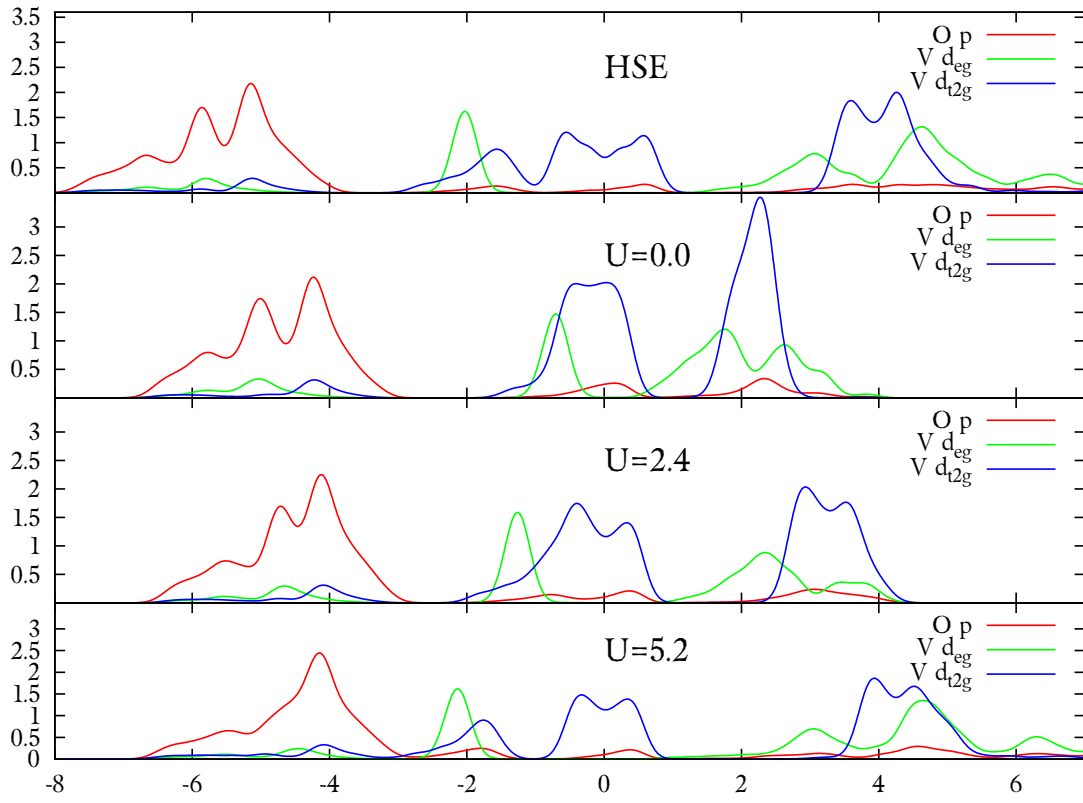
Figure 16: DOS of VO (100) monolayer (energy in eV)

disappear. This results in a high overall mean quadratic error, as can be seen in figure 21 in section 4.3.8. Data for CrO is given in table 15.
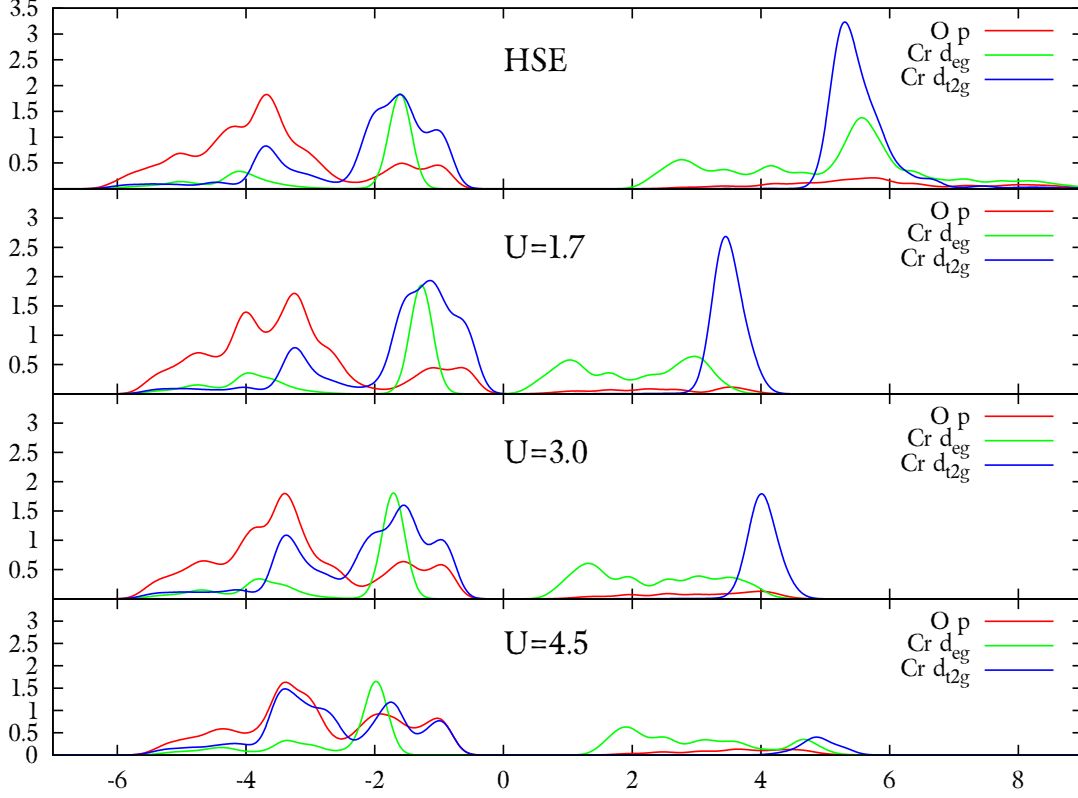
Figure 17: DOS of CrO (100) monolayer (energy in eV)

4.3.5 MnO

The good agreement of HSE06 and LDA+U can easily be seen with the naked eye in the case of MnO (figure 18) and the mean quadratic error is indeed very low (figure 21). Furthermore, all optimization processes for the valence bandwidth, the peak positions and all parameters combined yield the same U parameter, namely 4.1. Although MnO features a very low value of the DOS in a wide area around the Fermi energy, the actual HSE bandgap, with just 0.2 eV, is very small. Even for a high U value of 6.0 no gap is formed for the LDA+U functional, as can be concluded from fractional occupation numbers. Therefore a Δ of 0.2 eV has to be used. The typical behavior of the LDA+U functional can be very well observed in this case. The splitting of the d states of the Manganese ions is increased with increasing U. The Oxygen p states however remain

	$\mu\ [\mu_b]$	Gap [eV]
HSE06	3.733	3.051
U=0.0	3.634	0.0
U=1.7	3.726	0.0
U=3.0	3.784	1.579
U=4.5	3.839	2.352

Table 15: Data for CrO (100) monolayer

basically unchanged, about 1 eV too high in comparison to the DOS calculated with the HSE06 method. Data for the MnO monolayer is provided in table 16.
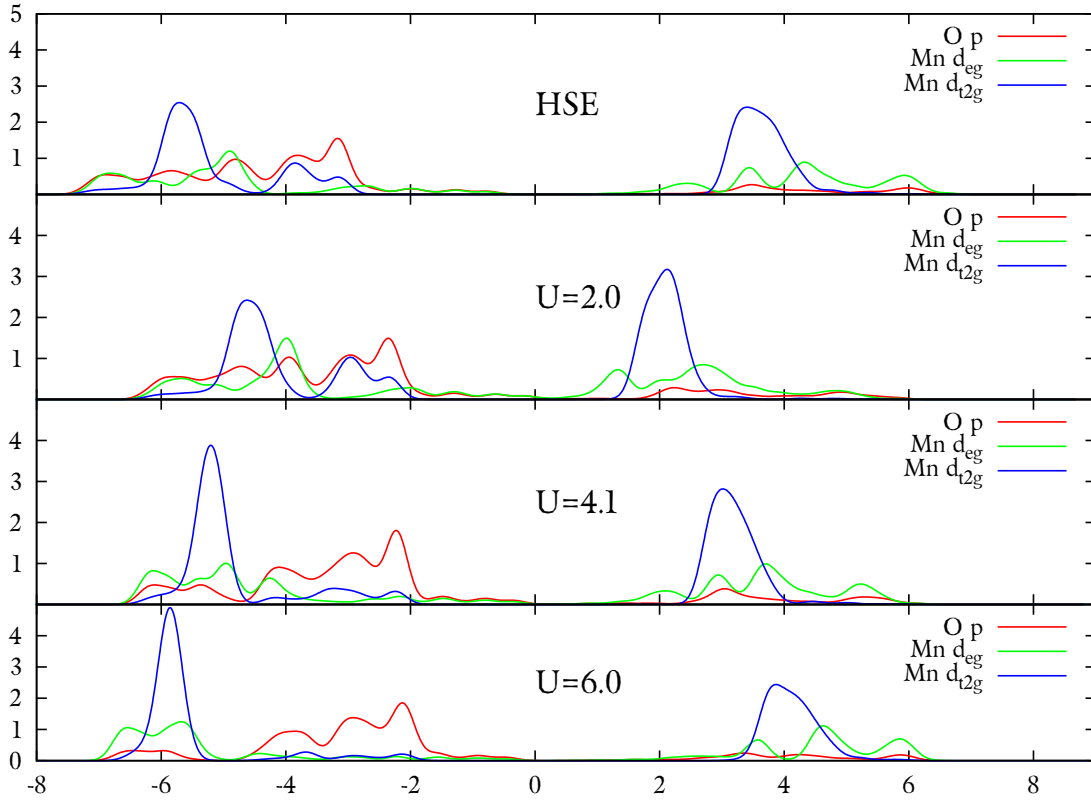
Figure 18: DOS of MnO (100) monolayer (energy in eV)

4.3.6 FeO

The general behavior of the LDA+U DOS of Iron monoxide for increasing values of U is not different to that of MnO. The d states are shifted away from the Fermi energy at

73

	μ $[\mu_b]$	Gap [eV]
HSE06	4.587	0.161
U=2.0	4.550	0.0
U=4.1	4.645	0.0
U=6.0	4.719	0.0

Table 16: Data for MnO (100) monolayer

both sides, but in the case of FeO, a gap is formed at $U = 2.3$. The optimization with respect to the valence bandwidth, as well as with respect to the peak positions lead to an ideal U value of 3.4, resulting in a needed Δ of 1.2 eV. For the overall optimization one gets $U = 4.4$ with a Δ of 1.1 eV. For this U parameter, the mean quadratic error is even lower as for MnO, as can be seen in figure 21. The HSE–LDA+U DOS comparison is shown in figure 19, and data is collected in table 17.
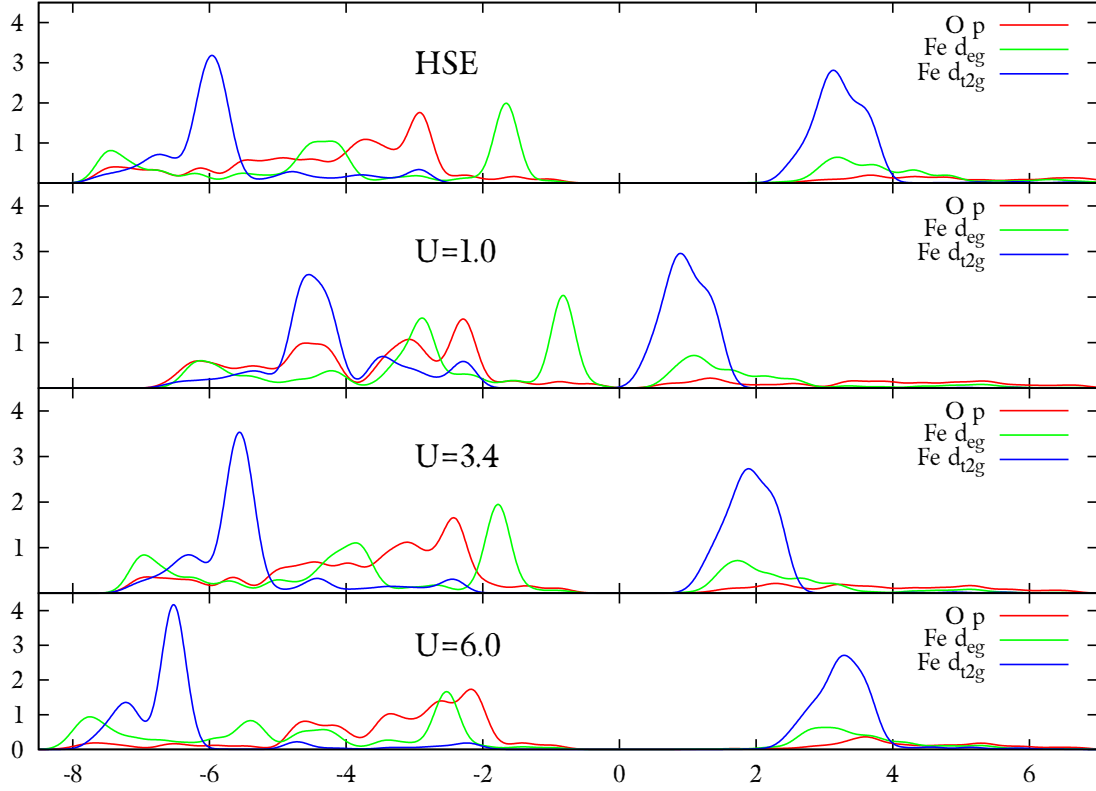
Figure 19: DOS of FeO (100) monolayer (energy in eV)

	μ [μ_b]	Gap [eV]
HSE06	3.741	2.613
U=1.0	3.649	0.0
U=3.4	3.745	1.408
U=4.4	3.779	1.513
U=6.0	4.719	1.663

Table 17: Data for FeO (100) monolayer

4.3.7 CoO

HSE06 yields a semiconductor with a bandgap of 2.4 eV for the (100) monolayer of Cobalt monoxide. The mean quadratic error of the LDA+U DOS, with respect to the HSE06 one, was found to be the lowest for all discussed monolayers (see figure 21). The overall optimization yields $U = 4.7$, which corresponds to a Δ value of 1.1 eV. For the valence bandwidth as well as for the peak positions, 4.1 is the best value for U, yielding also to a Δ of 1.1 eV. As it was the case for MnO and FeO as well, the top of the valence band of CoO has a large region of very low DOS. The HSE06 calculation yields a direct bandgap of 3.45 eV, just more than 1 eV larger than the fundamental gap. DOS graphs are given in figure 20 and data can be found in table 18.

	μ [μ_b]	Gap [eV]
HSE06	2.775	2.425
U=2.0	2.693	0.0
U=4.1	2.776	1.278
U=4.7	2.794	1.343
U=6.0	2.831	1.471

Table 18: Data for CoO (100) monolayer

4.3.8 Monolayer TMO Summary

In this section, the optimal U and Δ values, with respect to overall optimization, are summed up in table 19. If one compares this parameters to the bulk values in 11, the uniform enlargement of U is instantly visible. On average, the monolayer demands an
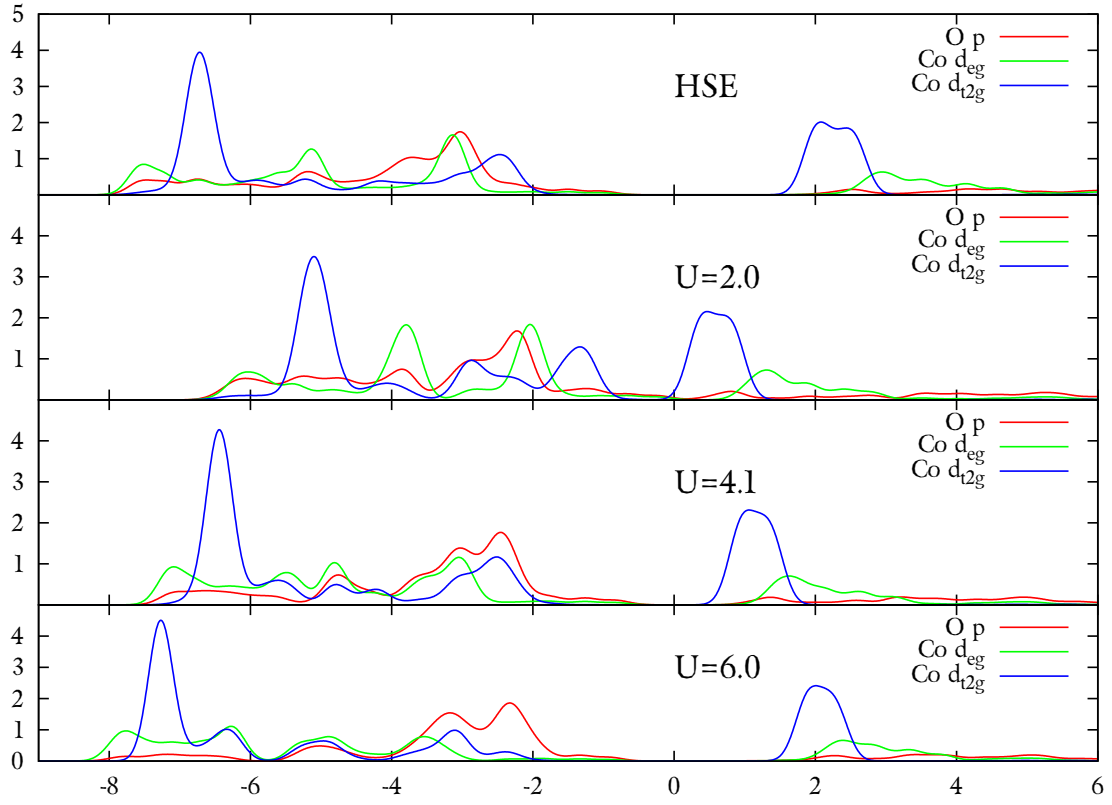
Figure 20: DOS of CoO (100) monolayer (energy in eV)

increase of U of about 2 eV, with only Manganese and Iron being lower than 1, namely 0.3 and 0.6 eV. The Δ parameter is usually smaller than for bulk configurations, with the exception of ScO and TiO, which are conducting in both configurations, and CrO, which is a conductor in the infinite crystal, but a semiconductor in the monolayer.

	ScO	TiO	VO	CrO	MnO	FeO	CoO
			Present work				
U [eV]	5.2	2.6	4.5	4.5	4.1	4.4	4.7
Δ [eV]	0.0	0.0	2.3	0.7	0.2	1.1	1.1

Table 19: Parameters U and Δ for (100) monolayer TMOs
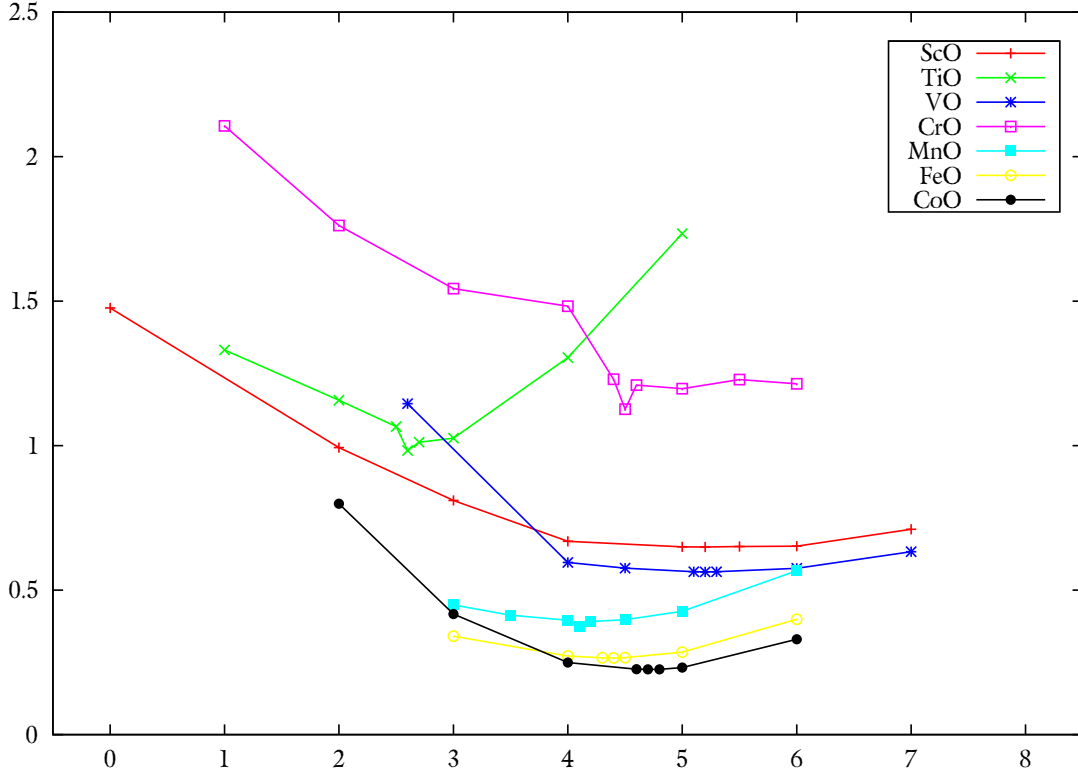
Figure 21: U dependent mean quadratic DOS error between HSE06 and LDA+U for monolayer TMOs. (U in eV on the x-axis, error in arbitrary units on the y-axis)

Figure 21 shows the mean quadratic error of the LDA+U calculations with respect to the HSE06 DOS for the U values given in table 19.

5 Summary and Conclusion

Eight $3d$ transition metal monoxides, ranging from ScO to NiO, were studied with two DFT based methods, the HSE06 functional and the LDA+U(+Δ) approach in their antiferromagnetic phases. The crystal structure used for bulk calculations was the ideal rocksalt structure, and if relaxations were performed, only the cell size was allowed to change, so no breaking of the symmetry was possible. Also a (100) monolayer, kept rigid at the bulk lattice constant, was analyzed for each TMO. All calculations were performed with the program package VASP, using PAW potentials provided in this package. The goal of this work on prototype systems was to provide reference points for the on-site interaction parameter U, with respect to the much more expensive HSE06 functional, for various transition metal compounds. To our best knowledge, no previous study compared these methods for such a wide range of materials, or included surface geometries.

The bulk HSE06 results match previous calculations and experiments quite well, were such data could be obtained (see tables 5, 7, 8, 9 and 10). It is therefore reasonable to conclude, that the hybrid functional approach serves also as a good standard for the optimization of the parameters U and Δ.

For the selection of the constants U and Δ, it was attempted to fit the electronic density of states from the LDA+U approach to the respective HSE benchmark. Hence, the DOS was first dissected into a valence and a conduction band and then into Oxygen p, transition metal d_{t2g} and transition metal d_{eg} states. The peak positions and the bandwidths were obtained by calculating the first and second moments of this functions. Now these 13 conditions, including the lattice parameter, were used to find values for U, that gave the best approximation for the given target. If a optimal U was found, Δ was selected in a fashion, that the LDA+U bandgap plus Δ was equal to the gap found with the HSE06 functional.

Compared to the parameters U and Δ from previous calculations, the values calculated in the present work differ in detail, but are of the same order of magnitude. Often quite different values for U are calculated for the same compound, depending on the parameters chosen for the optimization and so comparison to other results is complicated.

If one compares the bulk results with the monolayer parameters, one finds an increase of the on-site interaction parameter. This is to be expected, as the electrons are even more localized in the confines of the monolayer configuration. At the same time electron mobility is reduced as the DOS at the Fermi level decreases. (With the exception of CrO, which is metallic in bulk and a semiconductor in the monolayer.)

Concluding, one may argue that leaving the ab-initio confines in favor for the LDA+U approach with an adapted U parameter is a reasonable way of dealing with strongly localized electrons in large systems. However, only in a few cases does a single set of parameters describe the whole DOS well in respect to a HSE06 calculation. Usually one has to concentrate on a single aspect, e.g. the bandwidths, and the U chosen will than not approximate other aspects well. Therefore it is not generally advisable to use this method for predictions, but rather to serve as a model for a better understanding of the exchange interaction of a given system. A final list of all calculated data is given in table 20.

U optimized for		ScO	TiO	VO	CrO	MnO	FeO	CoO	NiO
				Bulk					
Lattice Constant	U	0.0	1.0	0.2	1.2	0.8	2.9	1.0	0.0
	Δ	0.0	0.0	2.9	0.0	2.9	2.2	3.5	4.4
Peak Positions	U	2.2	0.6	0.8	4.6	2.3	3.2	1.5	3.5
	Δ	0.0	0.0	2.9	0.0	1.5	2.2	3.5	2.0
Valence Bandwidths	U	1.5	0.0	0.5	0.0	1.4	3.5	2.2	3.5
	Δ	0.0	0.0	2.9	0.0	1.7	2.2	2.2	2.0
Overall	U	2.2	0.6	1.3	2.9	3.8	3.8	1.5	5.3
	Δ	0.0	0.0	2.9	0.0	1.3	2.2	3.5	1.3
				Monolayer					
Peak Positions	U	5.2	2.6	4.9	1.7	4.1	3.4	4.1	-
	Δ	0.0	0.0	0.0	3.1	0.2	1.2	1.1	-
Valence Bandwidths	U	6.1	2.5	0.0	0.0	4.1	3.4	4.1	-
	Δ	0.0	0.0	0.0	3.1	0.2	1.2	1.1	-
Overall	U	5.2	2.6	5.2	4.5	4.1	4.4	4.7	-
	Δ	0.0	0.0	0.0	0.7	0.2	1.1	1.1	-

Table 20: Calculated values U and Δ (in eV) for different optimizations.

List of Figures

List of Tables

References

[1] Karsten Held. Lecture notes on computational materials science, 2008.

[2] P. Hohenberg and W. Kohn. Inhomogeneous electron gas. *Phys. Rev.*, 136(3B):864, 1964.

[3] Mel Levy. Universal variational functionals of electron densities, first-order density matrices, and natural spin-orbitals and solution of the v-representability problem. *Proc. Natl. Acad. Sci.(USA)*, (76):6062–6065, 1979.

[4] W. Kohn and L. J. Sham. Self-consistent equations including exchange and correlation effects. *Phys. Rev.*, 140(4A):1133, 1965.

[5] M. Marder. *Condensed Matter Physics*. Wiley-Interscience.

[6] O. Gunnarsson, M. Jonson, and B. I. Lundqvist. Descriptions of exchange and correlation effects in inhomogeneous electron systems. *Phys. Rev. B*, 20(8):3136–3164, Oct 1979.

[7] R. Dreizler and E. Gross. *Density Functional Theory*. Plenum Press, New York, 1995.

[8] J.P. Perdew, J.A. Chevary, S.H. Vosko, K.A. Jackson, M.R. Pederson, D.J. Singh, and C. Fiolhais. Atoms, molecules, solids, and surfaces: Applications of the generalized gradient approximation for exchange and correlation. *Phys. Rev. B*, 46:6671, 1992.

[9] V. Ozoliņš and M. Körling. Full-potential calculations using the generalized gradient approximation: Structural properties of transition metals. *Phys. Rev. B*, 48(24):18304–18307, Dec 1993.

[10] C. Filippi, D. J. Singh, and C. J. Umrigar. All-electron local-density and generalized-gradient calculations of the structural properties of semiconductors. *Phys. Rev. B*, 50(20):14947–14951, Nov 1994.

[11] J.P. Perdew, J.A. Chevary, S.H. Vosko, K.A. Jackson, M.R. Pederson, D.J. Singh, and C. Fiolhais. Erratum: Atoms, molecules, solids, and surfaces: Applications of the generalized gradient approximation for exchange and correlation. *Phys. Rev. B*, 48:4978, 1993.

[12] J. P. Perdew, K. Burke, and M. Ernzerhof. Erratum: Generalized gradient approximation made simple. *Phys. Rev. Lett.*, 78:1396, 1997.

[13] Jochen Heyd, Gustavo E. Scuseria, and Matthias Ernzerhof. Hybrid functionals based on a screened coulomb potential. *J. Chem. Phys.*, 118(18):8207, 2003.

[14] Jochen Heyd, Gustavo E. Scuseria, and Matthias Ernzerhof. Erratum: Hybrid functionals based on a screened coulomb potential [j. chem. phys. 118, 8207 (2003)]. *J. Chem. Phys.*, 124:219906, 2006.

[15] Aliaksandr V. Krukau, Oleg A. Vydrov, Artur F. Izmaylov, and Gustavo E. Scuseria. Influence of the exchange screening parameter on the performance of screened hybrid functionals. *J. Chem. Phys.*, 125:224106, 2006.

[16] Vladimir I. Anisimov, Jan Zaanen, and Ole K. Andersen. Band theory and mott insulators: Hubbard U instead of stoner I. *Phys. Rev. B*, 44(3):943–954, Jul 1991.

[17] A. I. Liechtenstein, V. I. Anisimov, and J. Zaanen. Density-functional theory and strong interactions: Orbital ordering in mott-hubbard insulators. *Phys. Rev. B*, 52(8):R5467–R5470, Aug 1995.

[18] Lars Hedin. New method for calculating the one-particle green's function with application to the electron-gas problem. *Phys. Rev.*, 139(3A):A796–A823, Aug 1965.

[19] I. V. Solovyev and M. Imada. Screening of coulomb interactions in transition metals. *Phys. Rev. B*, 71(4):045103, Jan 2005.

[20] Matteo Cococcioni and Stefano de Gironcoli. Linear response approach to the calculation of the effective interaction parameters in the $LDA+U$ method. *Phys. Rev. B*, 71(3):035105, Jan 2005.

[21] F. Aryasetiawan, K. Karlsson, O. Jepsen, and U. Schönberger. Calculations of hubbard U from first-principles. *Phys. Rev. B*, 74(12):125106, Sep 2006.

[22] Nicholas J. Mosey and Emily A. Carter. Ab initio evaluation of coulomb and exchange parameters for $DFT+U$ calculations. *Phys. Rev. B*, 76(15):155123, Oct 2007.

[23] S. L. Dudarev, G. A. Botton, S. Y. Savrasov, C. J. Humphreys, and A. P. Sutton. Electron-energy-loss spectra and the structural stability of nickel oxide: An LSDA+U study. *Phys. Rev. B*, 57(3):1505–1509, Jan 1998.

[24] G. Kresse and J. Hafner. Ab initio molecular dynamics for liquid metals. *Phys. Rev. B*, 47:558, 1993.

[25] G. Kresse and J. Hafner. Ab initio molecular-dynamics simulation of the liquid-metal-amorphous-semiconductor transition in germanium. *Phys. Rev. B*, 49:14251, 1994.

[26] G. Kresse and J. Furthmüller. Efficiency of ab-initio total energy calculations for metals and semiconductors using a plane-wave basis set. *Comput. Mat. Sci.*, 6:15, 1996.

[27] G. Kresse and J. Furthmüller. Efficient iterative schemes for ab initio total-energy calculations using a plane-wave basis set. *Phys. Rev. B*, 54:11169, 1996.

[28] D. Vanderbilt. Soft self-consistent pseudopotentials in a generalized eigenvalue formalism. *Phys. Rev. B*, 41:7892, 1990.

[29] G. Kresse and J. Hafner. Norm-conserving and ultrasoft pseudopotentials for first-row and transition-elements. *J. Phys.: Condens. Matter*, 6:8245, 1994.

[30] P. E. Blöchl. Projector augmented-wave method. *Phys. Rev. B*, 50:17953, 1994.

[31] G. Kresse and D. Joubert. From ultrasoft pseudopotentials to the projector augmented-wave method. *Phys. Rev. B*, 59:1758, 1999.

[32] Georg Kresse, Martijn Marsman, and Jürgen Furthmüller. Vasp the guide. Technical report, Computational Physics, Faculty of Physics, Universität Wien, 2010.

[33] P. Mohn. *Magnetism in the Solid State.* Springer Series in Solid-State Sciences , Volume 134, 2003.

[34] J. Weiss. L'hypothèse du champ moléculaire et la propriété ferromagnétique. *J. de Physique*, 6(661), 1907.

[35] J.H. van Leeuwen. PhD thesis, Leiden.

[36] W. Heitler and F. London. Wechselwirkung neutraler Atome und homöopolare Bindung nach der Quantenmechanik. *Zeitschr. f. Physik*, 44(455), 1927.

[37] Elliott Lieb and Daniel Mattis. Theory of ferromagnetism and the ordering of electronic energy levels. *Phys. Rev.*, 125(1):164–172, Jan 1962.

[38] Werner Heisenberg. *Zeitschr. f. Physik*, 38(441), 1926.

[39] P. A. M. Dirac. On the theory of quantum mechanics. *Proc. Roy. Soc. A*, 112(661), 1926.

[40] Patrik Fazekas. *Lecture Notes on Electron Correlation and Magnetism.* World Scientific, 1999.

[41] H. A. Kramers. L'interaction entre les atomes magnétogènes dans un cristal paramagnétique. *Physica*, 1(182), 1934.

[42] C. G. Shull and J. Samuel Smart. Detection of antiferromagnetism by neutron diffraction. *Phys. Rev.*, 76(8):1256–1257, Oct 1949.

[43] P. W. Anderson. Antiferromagnetism. theory of superexchange interaction. *Phys. Rev.*, 79(2):350–356, Jul 1950.

[44] J. C. Slater. Ferromagnetism and the band theory. *Rev. Mod. Phys.*, 25(1):199–210, Jan 1953.

[45] D. R. Inglis. Non-orthogonal wave functions and ferromagnetism. *Phys. Rev.*, 46(2):135–138, Jul 1934.

[46] W. J. Carr. Use of non-orthogonal wave functions in the treatment of solids, with applications to ferromagnetism. *Phys. Rev.*, 92(1):28–35, Oct 1953.

[47] P. W. Anderson. New approach to the theory of superexchange interactions. *Phys. Rev.*, 115(1):2, Jul 1959.

[48] J. Yamashita and J. Kondo. Superexchange interaction. *Phys. Rev.*, 109(3):730–741, Feb 1958.

[49] J. M. D. Coey. *Magnetism and magnetic materials*. Cambridge University Press, 2010.

[50] Ralph W. G. Wyckoff. *Crystal Structures*. Interscience Publishers New York, second edition, 1963.

[51] A. F. Holleman and E Wiberg. *Inorganic Chemistry*. San Diego: Academic Press, 2001.

[52] Norman N. Greenwood and A. Earnshaw. *Chemistry of the Elements*. Oxford: Butterworth-Heinemann, 2 edition, 1997.

[53] P. S. Silinsky and Mohindar S. Seehra. Principal magnetic susceptibilities and uniaxial stress experiments in CoO. *Phys. Rev. B*, 24(1):419–423, Jul 1981.

[54] C. Rödl, F. Fuchs, J. Furthmüller, and F. Bechstedt. Quasiparticle band structures of the antiferromagnetic transition-metal oxides MnO, FeO, CoO, and NiO. *Phys. Rev. B*, 79(23):235114, 2009.

[55] F. Rivadulla, J. Fernández-Rossier, M. García-Hernández, M. A. López-Quintela, J. Rivas, and J. B. Goodenough. Vo: A strongly correlated metal close to a mott-hubbard transition. *Phys. Rev. B*, 76(20):205110, Nov 2007.

[56] William C. Mackrodt, Derek S. Middlemiss, and Thomas G. Owens. Hybrid density functional theory study of vanadium monoxide. *Phys. Rev. B*, 69(11):115119, Mar 2004.

[57] E. Engel and R. N. Schmid. Insulating ground states of transition-metal monoxides from exact exchange. *Phys. Rev. Lett.*, 103(3):036404, Jul 2009.

[58] Deepa Kasinathan, J. Kuneš, K. Koepernik, Cristian V. Diaconu, Richard L. Martin, Ionuţ D. Prodan, Gustavo E. Scuseria, Nicola Spaldin, L. Petit, T. C. Schulthess, and W. E. Pickett. Mott transition of MnO under pressure: A comparison of correlated band theories. *Phys. Rev. B*, 74(19):195110, Nov 2006.

[59] Fabien Tran, Peter Blaha, Karlheinz Schwarz, and Pavel Novák. Hybrid exchange-correlation energy functionals for strongly correlated electrons: Applications to transition-metal monoxides. *Phys. Rev. B*, 74(15):155108, Oct 2006.

[60] W. L. Roth. Magnetic structures of MnO, FeO, CoO, and NiO. *Phys. Rev.*, 110(6):1333–1341, Jun 1958.

[61] W. Jauch and M. Reehuis. Electron density distribution in paramagnetic and antiferromagnetic MnO: A γ-ray diffraction study. *Phys. Rev. B*, 67(18):184420, May 2003.

[62] A. K. Cheetham and D. A. O. Hope. Magnetic ordering and exchange effects in the antiferromagnetic solid solutions $Mn_xNi_{1-x}O$. *Phys. Rev. B*, 27(11):6964–6967, Jun 1983.

[63] J. van Elp, R. H. Potze, H. Eskes, R. Berger, and G. A. Sawatzky. Electronic structure of MnO. *Phys. Rev. B*, 44(4):1530–1537, Jul 1991.

[64] J. van Elp. PhD thesis, University of Groningen.

[65] W. Jauch, M. Reehuis, H. J. Bleif, F. Kubanek, and P. Pattison. Crystallographic symmetry and magnetic structure of CoO. *Phys. Rev. B*, 64(5):052102, Jul 2001.

[66] S. Hüfner, J. Osterwalder, T. Riesterer, and F. Hulliger. Photoemission and inverse photoemission spectroscopy of NiO. *Solid State Commun.*, 52(793), 1984.

[67] G. A. Sawatzky and J. W. Allen. Magnitude and origin of the band gap in NiO. *Phys. Rev. Lett.*, 53(24):2339–2342, Dec 1984.

Acknowledgement

I want to thank Prof. Josef Redinger for the interresting topic and the support he gave me throughout the whole working process. Not only did he help with any physics question that came up, but he was also always ready to solve computer problems or provided other useful knowledge. I am also very grateful that Prof. Peter Mohn gave me the opportunity to start working in the CMS group in 2009, leading ultimately to this thesis. Robert Hammerling always encouraged me to think deeply about the physics background of every calculation and provided me with more books and papers than I could read, which I appreciated very much. I would also like to thank him for proofreading this thesis and his comments and suggestions for improvement. Without the friendship of my colleague Franz Schmidt all my academic studies would have been that much harder and I am not sure if I ever would have come to the point of finishing my thesis. There can be no doubt that he was the most important person in my life as a physicist so far. Most of all though, I would like to thank Robert Achleitner, Pedro Osvaldo Bedolla Velázquez, Andreas Garhofer and Christoph Gruber. It was a pleasure to share a work environment with you guys and I can not begin to imagine how I should have finished this work without your support.

It would have been impossible for me to study physics without the encouragement and support I received from my family and so the long list of things I am thankful for to them is growing even longer. Finally I want to thank all my friends, who somehow managed to keep me sane and even happy in the last two stressful months.